Metabolic Engineering 72 (2022) 337–352

Contents lists available at ScienceDirect

Metabolic Engineering

journal homepage: www.elsevier.com/locate/meteng

Biobased PET from lignin using an engineered *cis, cis*-muconate-producing Pseudomonas putida strain with superior robustness, energy and redox properties

Michael Kohlstedt [a], Anna Weimer [a], Fabia Weiland [a], Jessica Stolzenberger [a], Mirjam Selzer [a], Miguel Sanz [b], Laurenz Kramps [b], Christoph Wittmann [a,*]

[a] Institute of Systems Biotechnology, Saarland University, Saarbrücken, Germany
[b] Taros Chemicals GmbH, Dortmund, Germany

ARTICLE INFO

Dedicated to Judith Becker (* 2.2.1981, † 27.4.2021), a gifted metabolic engineer of sustainable cell factories and our cherished colleague and friend at the Institute of Systems Biotechnology of Saarland University

Keywords:
Pseudomonas putida
Lignin
PET
Catechol
^{13}C metabolic Flux analysis
Transcriptomics
ATP
NADPH
PQQH2
FADH2
Genome reduction
EM42

ABSTRACT

Polyethylene terephthalate (PET), the most common synthetic polyester today, is largely produced from fossil resources, contributing to global warming. Consequently, sustainable sources must be developed to meet the increasing demand for this useful polymer. Here, we demonstrate a cascaded value chain that provides green PET from lignin, the world's most underutilized renewable, via fermentative production of *cis, cis*-muconate (MA) from lignin-based aromatics as a central step. Catechol, industrially the most relevant but apparently also a highly toxic lignin-related aromatic, strongly inhibited MA-producing *Pseudomonas putida* MA-1. Assessed by ^{13}C metabolic flux analysis, the microbe substantially redirected its carbon core fluxes, resulting in enhanced NADPH supply for stress defense but causing additional ATP costs. The reconstruction of MA production in a genome-reduced *P. putida* chassis yielded novel producers with superior pathway fluxes and enhanced robustness to catechol and a wide range of other aromatics. Using the advanced producer *P. putida* MA-10 catechol, MA could be produced in a fed-batch process from catechol (plus glucose as additional growth substrate) up to an attractive titer of 74 g L^{-1} and a space-time-yield of 1.4 g L^{-1} h^{-1}. In terms of co-consumed sugar, the further streamlined strain MA-11 achieved the highest yield of 1.4 mol MA (mol glucose)$^{-1}$, providing a striking economic advantage. Following fermentative production, bio-based MA was purified and used to chemically synthetize the PET monomer terephthalic acid and the comonomer diethylene glycol terephthalic acid through five steps, which finally enabled the first green PET from lignin.

1. Introduction

Polyethylene terephthalate (PET), a clear, strong, and lightweight thermoplastic, is the most common synthetic polyester produced today (Geyer, 2020). Introduced in 1957 by DuPont, more than 82 million metric tons of PET are produced globally each year from petroleum to make single-use beverage bottles, packaging, clothing, and carpets. Given its multiple uses, PET, polymerized from the two monomers terephthalic acid and ethylene glycol, is regarded as the most useful plastic worldwide. Over the past few years, great progress has been made to tackle the relatively labile chemical bonds of the polymer towards chemical and, more recently, biological, recycling and upcycling (Rorrer et al., 2019; Sadler and Wallace, 2021; Singh et al., 2021; Tiso et al., 2021; Tournier et al., 2020; Werner et al., 2021). Flanked by efforts from the industry to make stronger use of recycled and reprocessed PET, these achievements are strong drivers toward a greener PET industry. Nevertheless, PET is still produced from fossil resources, which is why manufacturing of this prevalent plastic considerably contributes to global warming. Promising approaches toward a more sustainable PET industry employ biobased ethylene glycol, which is accessible through hydrogenolysis of sorbitol from renewable resources (Pang et al., 2016). To date, however, terephthalic acid, contributing 80% to PET carbon, is still derived from fossil fuels.

Several routes for terephthalic acid production from biomass have

* . Corresponding author. Campus A1 5, 66123, Saarbrücken, Germany.
E-mail address: christoph.wittmann@uni-saarland.de (C. Wittmann).

https://doi.org/10.1016/j.ymben.2022.05.001
Received 12 March 2022; Received in revised form 18 April 2022; Accepted 4 May 2022
Available online 8 May 2022

been proposed to achieve a 100% biobased PET (Collias et al., 2014). One such method is the chemical transformation of *trans, trans*-muconic acid, the isomer of *cis, cis*-muconic acid (MA), into terephthalic acid. In this regard, fermentative MA could serve as a sustainable building block for bio-PET. Particularly promising is the production of MA from aromatics, accessible through depolymerization of lignin (Almqvist et al., 2021), the most undervalued waste stream worldwide (Becker and Wittmann, 2019). Lignin itself accumulates in massive amounts from large-scale lignocellulosic biorefineries and pulp and paper industries but is simply burned in most cases (Weiland et al., 2021). Additionally, recurring, different agricultural residues display a massive source for lignin upgrading, altogether potentially providing up to 200 million tons of lignin for upgrading every year (Goncalves et al., 2020).

Notably, *Pseudomonas putida*, a promising candidate for microbial lignin valorization (Bugg et al., 2021), can produce MA through fermentation and has been studied intensively over the past few years in this regard (Johnson et al., 2016; Kohlstedt et al., 2018; van Duuren et al., 2012; Vardon et al., 2015). To date, however, biobased MA production from lignin-based aromatics still remains to be optimized (Khalil et al., 2020). Despite great efforts to engineer *P. putida*, product titers have remained relatively low (Weiland et al., 2021) in comparison to other dicarboxylic acids accessible through fermentation (Becker et al., 2015; Lange et al., 2017; Rohles et al., 2018). Currently, this limitation displays a major bottleneck toward industrial applicability. A main challenge seems to be the variable mechanisms of toxicity of different aromatic substrates that are known to disrupt cell membranes (Lou et al., 2012), provoke oxidative stress and uncouple oxidative phosphorylation (Imlay, 2013; Nikel et al., 2021). This phenomenon might explain why *P. putida* loses performance during MA production in fed-batch experiments (Kohlstedt et al., 2018). Compounded toxicity effects, expectable when using aromatic mixtures (Weiland et al., 2021) and the built-up of toxic pathway intermediates during production (Kohlstedt et al., 2018), pose even bigger challenges.

Here, we show that catechol-stressed *P. putida* rearranges its central carbon metabolism and thereby sacrifices ATP generation to enhance NADPH supply for stress defense, and that a range of transcriptional changes are associated to this adaptation. These findings inspired the construction of MA-producing mutants based on *P. putida* EM42, a genome-reduced derivative of KT2440 (Martínez-García et al., 2014) that was previously shown to generate elevated levels of ATP and NADPH from glucose due to its increased anabolic productivity (Lieder et al., 2015; Martínez-García et al., 2014). The created, novel genome-reduced MA producers *P. putida* MA-10 and MA-11 exhibited higher tolerance against a range of aromatics, enabled by a more efficient pathway use under stress. When benchmarked in fed-batch processes on catechol, the technically most relevant but apparently also most toxic lignin-associated aromatic, the novel strains were found to be superior to their KT 2440 counterparts in MA titer, production rate, and the need for additional. Following fermentation, biobased MA was purified and used to chemically synthetize the PET monomer terephthalic acid and the comonomer diethylene glycol terephthalic acid, finally enabling green PET synthesis from lignin for the first time.

2. Materials and methods

2.1. Strains and plasmids

P. putida KT2440 (Stephan et al., 2006), its MA-producing derivatives *P. putida* Δ*catBC* (MA-1) and Δ*catBC* catA2 (MA-6), and the integrative plasmids pEMG:catBC and pEMG-P_{catA} catA2 were obtained from previous work (Kohlstedt et al., 2018). The genome-reduced chassis strain *P. putida* EM42, derived from strain KT2440 (Martínez-García et al., 2014), was kindly donated by Esteban Martinez-Garcia and Victor de Lorenzo (National Biotechnology Centre, Madrid, Spain). *Escherichia coli* DH5α (Invitrogen, Carlsbad, CA, USA) and *E. coli* DH5α λpir (Biomedal Life Science, Seville, Spain) were obtained for cloning purposes. For maintenance, cells were stored in 15% (v/v) glycerol at −80 °C. All strains of this work are listed in Table 1.

2.2. Genetic engineering

P. putida EM42 was genetically engineered using the pEMG/pSW-I system(Martínez-García and de Lorenzo, 2011) (Table 1). Briefly, the integrative plasmid pEMG:catBC was used for simultaneous deletion of muconate cycloisomerase (*catB*) and muconolactone Δ-isomerase (*catC*) (bp 4,238,924–4,236,524) (Kohlstedt et al., 2018). The plasmid pEMG-P_{catA} catA2 was used to integrate a second catechol 1,2-dioxygenase gene, i.e., *catA2* (PP_3166), into the *cat* operon under the control of the native P_{cat} promoter downstream of *catA* (bp 4,235,832) (Kohlstedt et al., 2018). Mutants obtained after the second recombination were validated for the desired genomic modification by PCR and by sequencing.

2.3. Media

Cells were grown in modified E2 glucose medium (Hartmans et al., 1989) that contained 7.5 g of glucose, 2 g of $(NH_4)_2SO_4$, 7.55 g of K_2HPO_4, 4.25 g of $NaH_2PO_4 \bullet 2H_2O$, 0.1 g of $MgCl_2 \bullet 6H_2O$, 10 mg of EDTA, 5 mg of $FeSO_4 \bullet 7H_2O$, 1 mg of $CaCl_2 \bullet 2H_2O$, and 1 mL of 1000x trace element stock solution (2 g of $ZnSO_4 \bullet 7H_2O$, 1 g of $MnCl_2 \bullet 2H_2O$, 0.4 g of $CoCl_2 \bullet 6H_2O$, 0.3 g of $Na_2B_4O_7 \bullet 10H_2O$, 0.2 g of $Na_2MoO_4 \bullet 2H_2O$, 0.2 g of $CuSO_4 \bullet 5H_2O$, and 0.2 g of $NiCl_2 \bullet 6H_2O$) per liter. The pH value of the medium was adjusted to 7.0 using 6 M NaOH. For agar plate cultures, 15 g L^{-1} agar (Becton and Dickinson, Heidelberg, Germany) was added. In tolerance test experiments, selected aromatics were added to the medium as described below. In isotopic tracer experiments for ^{13}C metabolic flux analysis, glucose was replaced in parallel setups either by (i) 99% [1–^{13}C] glucose (Sigma–Aldrich, Taufkirchen, Germany), (ii) 99% [6–^{13}C] glucose (Omicron Inc., South Bend, OH, USA), or (iii) an equimolar mixture of naturally labeled and 99% [$^{13}C_6$] glucose (Euriso-top, Saclay, France)(Kohlstedt and Wittmann, 2019).

2.4. Tolerance testing of cells against lignin-relevant aromatics

To test the tolerance of *P. putida* strains against selected lignin-relevant aromatics, cultivations were carried out in 48-well flower plates in a Biolector bioreactor system with online sensing of cell growth (Beckman Coulter GmbH, Baesweiler, Germany). Each well was filled with 1 mL of E2 glucose medium. Hereby, the following selected aromatics were added to the medium from sterilized stocks (pH 7.0) to

Table 1
Strains and plasmids used in this study.

Strain	Genotype	Reference
E. coli		
DH5α	*supE44, ΔlacU169 (φ80 lacZΔM15), hsdR17 (rk-mk+), recA1, endA1, thi1, gyrA, relA*	Invitrogen, Carlsbad, CA, USA
DH5α λpir	*λpir* lysogen of DH5α	Biomedal Life Sciences, Seville, Spain
P. putida		
KT2440	wild type	Nelson et al. (2002)
MA-1	KT2440 Δ*catBC*	Kohlstedt et al. (2018)
MA-6	MA-1 P_{cat} *catA-catA2*	Kohlstedt et al. (2018)
EM42	KT2440 derivative: Δprophages1,2,3,4 ΔTn7 Δ*endA1* Δ*endA2* Δ*hsdRMS* Δflagellum ΔTn*4652*	Martínez-García et al. (2014)
MA-10	EM42 Δ*catBC*	This study
MA-11	MA-10 P_{cat} *catA-catA2*	This study
Plasmids		
pEMG	Km^R, *oriR6K*, *lacZα* with two flanking I-SceI sites	Martínez-García and de Lorenzo (2011)
pSW-I	*oriV* (RK2), *xylS*, P_m→I-SceI; Ap^R	Wong and Mekalanos (2000)

assess their impact on cell growth: benzoate (0–75 mM), caffeate (0–25 mM), catechol (0–15 mM), *p*-coumarate (0–30 mM), guaiacol (0–15 mM), phenol (0–20 mM), protocatechuate (0–60 mM), syringol (0–15 mM), and vanillate (0–45 mM). The cultures were inoculated with cells obtained from a preculture in 10 mL of E2 glucose medium in 100 mL baffled shake flasks, incubated on a rotary shaker (30 °C, 230 rpm, Multifors, Infors AG, Bottmingen, Switzerland), harvested during exponential growth (8000×*g*, 5 min, 4 °C), and washed once with fresh medium. Biolector cultures were grown for 48 h at 30 °C, 1,300 rpm, and 85% humidity. Cell growth was monitored online as the optical density (OD_{620}) against cell-free medium as a reference. Afterward, the lag phase and maximum specific growth rate were estimated from the growth data for each condition. The latter was determined during the exponential growth phase by regression of ln (OD_{620}) over time. All experiments were performed in biological duplicate.

2.5. MA production in shake flasks

A single colony from a fresh agar plate was used to inoculate a preculture (10 mL E2 glucose medium in a 100 mL baffled shake flask), which was then incubated on a rotary shaker (30 °C, 230 rpm, Multifors, Infors AG). Cells were harvested during exponential growth (8000×*g*, 5 min, 4 °C), washed once with fresh E2 glucose medium, and used to inoculate the main culture (50 mL of E2 glucose medium in a 500 mL baffled shake flask). For MA production, selected aromatic substrates were added from sterilized stocks at the beginning of the cultivation as given below. All experiments were conducted with three biological replicates.

2.6. ^{13}C tracer cultivations for metabolic flux analysis

A single colony was transferred from an agar plate into 10 mL of E2 glucose medium in a baffled shake flask (100 mL). Cells were then incubated overnight at 30 °C and 230 rpm on a rotary shaker (Multifors, Infors AG), collected by centrifugation (8000×*g*, 5 min, 4 °C), washed once in glucose-free medium, and used to inoculate the tracer experiments. Hereby, the initial optical density (OD_{600}) was kept below 0.02 (<1% of the cell concentration sampled for later ^{13}C labeling analysis) to avoid interference of unlabeled biomass with ^{13}C labeling patterns (Wittmann, 2007). Three parallel setups with different ^{13}C glucose tracers (25 mL of medium in 250 mL baffled shake flasks) were chosen to resolve the different pathways and cycles in the biochemical network of *P. putida*(Kohlstedt and Wittmann, 2019). The three cultures also provided physiological parameters on rates and yields (Table 2). For ^{13}C labeling analysis, cell pellets were harvested at different time points during exponential growth, reflecting cell concentrations between OD 2 and 5 (Kohlstedt and Wittmann, 2019).

2.7. Fed-batch production of MA

The production performance of MA-producing *P. putida* KT2440 strains was evaluated in a fed-batch process. Two different operation modes were tested: a *yield-oriented* and a *rate-oriented* scenario. In both cases, fermentation was carried out in 1 L DASGIP bioreactors (Eppendorf, Jülich, Germany) at 30 °C and pH 7.0 using glucose as a carbon source for growth and catechol as a lignin monomer for MA production. The initial E2 batch medium contained the following per liter: 1.8 g of glucose, 15 g of $(NH_4)_2SO_4$, 1.55 g of K_2HPO_4, 0.85 g of $NaH_2PO_4•2H_2O$, 1.0 g of $MgCl_2•6H_2O$, 10 mg of EDTA, 10 mg of $FeCl_3•6H_2O$, 5 mg of $FeSO_4•7H_2O$, 1 mg of $CaCl_2•2H_2O$, 1 mL of the abovementioned trace element solution, and 200 mg of Antifoam 204 (Sigma–Aldrich, Taufkirchen, Germany). The reactors were inoculated with the corresponding strain at an initial OD_{600} of 0.1, whereby preculture incubation and inoculum preparation were performed as described above. The initial aeration rate was set to 1 vvm, and pressurized air was used. Later, the dissolved oxygen (DO) level was maintained above 50% by adjusting the stirrer speed and aeration rate and (when needed) by adding pure oxygen.

The *yield-oriented* scenario aimed to provide the cells with sufficient glucose plus noninhibitory shots of catechol. After the batch phase, which was started with an initial volume of 490 mL, glucose and other nutrients were added exponentially. The concentrated feed contained 600 g of glucose, 50 g of $(NH_4)_2SO_4$, 1.55 g of K_2HPO_4, 0.85 g of $NaH_2PO_4•2H_2O$, 10 g of $MgCl_2•6H_2O$, 50 mg of EDTA, 50 mg of $FeCl_3•6H_2O$, 5 mg of $FeSO_4•7H_2O$, 5 mg of $CaCl_2•2H_2O$, 10 mL of the abovementioned trace element solution, and 200 mg of Antifoam 204 (Sigma–Aldrich). The feed rate (F) was based on the desired specific growth rate ($\mu_{set} = 0.04\ h^{-1}$), the biomass yield of unstressed *P. putida* on glucose ($Y_{X/S} = 0.4\ g\ g^{-1}$), and the maintenance coefficient ($m_s = 0.037\ g\ g^{-1}\ h^{-1}$) (van Duuren et al., 2013) (Eq. (1)):

$$F = \left(\frac{\mu_{set}}{Y_{x/S}} + m_s \cdot e^{0.02\ (t-t_0)}\right) \cdot \frac{V_L X_0 e^{\mu_{set}\ (t-t_0)}}{S_0} \quad (1)$$

The latter was empirically set to increase with time to compensate for the expected steadily growing metabolic burden. Other considered parameters were the reactor liquid volume V_L, the biomass concentration at the beginning of the feed phase X_0, and the glucose concentration of feed S_0. The process was operated as a pH-stat, which coupled the addition of catechol to the automatic pH control (van Duuren et al., 2012; Wittmann et al., 1995). Hereby, catechol (2.5 M) and NaOH (6 M) were connected as separate solutions. Prior to fermentation, the catechol feed was degassed using nitrogen to prevent oxidation. Using this setup, catechol was then added in noninhibitory shots and remained below a maximum level of 0.5 mM.

The *rate-oriented scenario* challenged the cells with inhibitory shots of catechol, while the glucose supply remained the same. The following modifications were made to the cultivation setup: (i) the use of a lower volume of batch medium (300 mL) with increased buffer capacity (7.55 g L^{-1} K_2HPO_4, 4.25 g L^{-1} $NaH_2PO_4 • 2H_2O$) and glucose level (7.5 g L^{-1}), (ii) the use of more concentrated feeds of catechol (4 M) and NaOH (9 M), and (iii) the addition of 1 mol% benzoic acid to the catechol feed to increase the conversion rate (Kohlstedt et al., 2018). Glucose and other nutrients were added exponentially as given above. Hereby, the addition of catechol was coupled to the DO signal. Once the DO level surpassed a predefined set-point, catechol was automatically added to the experimentally determined strain-specific mean inhibitory concentration. For this purpose, the catechol feed pumps were specifically programmed for each strain using VBA scripting, built in DASGIP control

Table 2
Physiological comparison between wild-type *P. putida* KT2440 and EM42 under reference and catechol-degrading conditions: The data shown comprise the specific growth rate (μ), the specific glucose uptake rate (q_{Glc}), the biomass yield ($Y_{X/Glc}$), and the secretion rates for gluconate (q_{GA}) and 2-ketogluconate (q_{2KGA}). Values represent the mean and standard deviation of 3 biological replicates and were determined during the exponential growth phase using linear regression.

Genotype	Condition	μ [h^{-1}]		q_{Glc} [mmol g_{DCW}^{-1} h^{-1}]		$Y_{X/Glc}$ [g_{DCW} mol^{-1}]		q_{GA} [mmol g_{DCW}^{-1} h^{-1}]		q_{2KGA} [mmol g_{DCW}^{-1} h^{-1}]	
MA1 (KT2440 *ΔcatBC)*	–	0.53	± 0.02	6.63	± 0.19	80.1	± 6.1	0.27	± 0.07	0.12	± 0.06
	5 mM catechol	0.42	± 0.02	5.39	± 0.40	78.5	± 3.1	0.08	± 0.04	0.07	± 0.02
MA10 (EM42 *ΔcatBC)*	–	0.56	± 0.01	5.06	± 0.14	111.2	± 3.6	0.19	± 0.01	0.18	± 0.01
	5 mM catechol	0.38	± 0.01	3.57	± 0.14	106.7	± 2.8	0.06	± 0.04	<0.01	± 0.00

software. All fermentations were conducted in duplicate.

2.8. Quantification of cells, substrates, and products

The cell concentration was monitored spectrophotometrically at 600 nm (OD_{600}). An experimentally determined correlation factor of 0.54 g L^{-1} OD^{-1} was used for conversion of OD_{600} into dry cell weight (Kohlstedt et al., 2018). The glucose level was quantified by HPLC (1260 Infinity Series, Agilent, Darmstadt, Germany) using a MetaCarb 87C column (Agilent) as the stationary phase, deionized water at 80 °C and a flow rate of 1 mL min^{-1} as the mobile phase, and refractive index detection. Gluconate and 2-ketogluconate were quantified by HPLC (1260 Infinity Series, Agilent) using an Aminex HPX-87H column (Bio–Rad, Hercules, CA, USA) at 65 °C, isocratic elution with 50 mM H_2SO_4 at a flow rate of 0.5 mL min^{-1}, and UV detection at 210 nm. Aromatics and MA were quantified by HPLC as described previously (Barton et al., 2018).

2.9. GC-MS labeling analysis of biomass constituents

Sampling, sample processing, and GC-MS-based ^{13}C labeling analysis of biomass constituents was carried out as described previously (Kohlstedt and Wittmann, 2019). To assess the ^{13}C labeling pattern of proteinogenic amino acids, cells sampled from the corresponding ^{13}C tracer cultures were first hydrolyzed (6 M HC, 24 h, 100 °C). The obtained hydrolysates were filtered, dried under a nitrogen stream, and derivatized using *N-methyl-N-tert*-butyldimethylsilyl-trifluoroacetamide (Macherey-Nagel, Düren, Germany). The mass isotopomer distributions (MIDs) of the available proteinogenic amino acids were then measured by GC-MS (7890B GC, 5977A MS, Agilent Technologies, Waldbronn, Germany). All samples were first analyzed in scan mode to check for potential isobaric interference of the analytes of interest with the sample matrix (Wittmann, 2007). Subsequently, the ^{13}C labeling patterns of the amino acids were measured at selected ion clusters using selective ion monitoring (SIM) (Kohlstedt and Wittmann, 2019). Additional ^{13}C labeling information was obtained from the analysis of cellular glycogen and glucosamine, reflecting the labeling pattern of their metabolic precursors, glucose 6-phosphate (G6P) and fructose 6-phosphate (F6P), respectively. Therefore, biomass was hydrolyzed (2 M HCl, 2 h, 100 °C), filtered, dried and derivatized in a two-step procedure: methoximation using methoxylamine followed by silylation using *N,O*-bis--trimethylsilyl-trifluoroacetamide (Macherey-Nagel) at 80 °C for 30 min. MIDs were obtained from two glycogen-derived glucose fragments, representing the G6P pool ($[C_1–C_6]$ *m/z* 554–560, $[C_3–C_6]$ *m/z* 319–323) and three glucosamine fragments ($[C_1–C_6]$ *m/z* 553–559, $[C_3–C_6]$ *m/z* 319–323, $[C_1–C_2]$ *m/z* 159–161) stemming from F6P (Kohlstedt and Wittmann, 2019).

2.10. Metabolic flux estimation

The biochemical reaction network of *P. putida* was taken from previous work (Kohlstedt and Wittmann, 2019) and is given in Table S1 (supplementary file 1). For each strain, 534 MIDs, obtained from three parallel experiments on the different ^{13}C tracers, were used for flux calculation. The metabolic and isotopic steady state for each culture was experimentally verified by checking for constant ^{13}C labeling patterns and constant growth kinetics and stoichiometry over time (Becker et al., 2008). Metabolic fluxes were estimated using the open source software OpenFLUX 2.1 (Quek et al., 2009) and MATLAB (Mathworks, Natick, USA) (Kohlstedt et al., 2014), considering growth stoichiometry (Table 2), anabolic precursor demand (Table S2, supplementary file 1), and ^{13}C labeling data (Table S3, Table S4, supplementary file 1). Prior to the simulation, the experimentally determined mass distributions were corrected for naturally occurring isotopes (van Winden et al., 2002) using a built-in algorithm of OpenFLUX. As the contribution of the 2-ketogluconate loop was not resolvable by ^{13}C tracing, the flux split at the periplasmic gluconate pool was constrained by the activity ratio of the two kinases (GnuK and KguK) of the gluconate bypass (GnuK) and the 2-ketogluconate loop (KguK) (Kohlstedt and Wittmann, 2019; Nikel et al., 2015, 2021; Tlemcani et al., 2008). Kinase activities were measured as described previously (Kohlstedt and Wittmann, 2019). Multiple parameter estimations with statistically varied starting values confirmed the identification of global minima. After flux parameter estimation, 95% confidence intervals were determined by Monte-Carlo sensitivity analysis (Wittmann and Heinzle, 2002).

2.11. Redox and energy balancing

The estimated fluxes (see above) allowed for a quantitative inspection of redox and energy metabolism. Regarding redox power, the supply of NADPH, NADH, $PQQH_2$, and $FADH_2$ was calculated from the corresponding cofactor-forming fluxes, considering the recently determined cofactor specificities under *in vivo* conditions in *P. putida* (Nikel et al., 2015). The anabolic NADPH requirement and anabolically produced NADH were estimated from the biomass composition (van Duuren et al., 2013) and the measured specific growth rates (Table 2). Regarding cellular energy, the production of ATP via substrate-level phosphorylation (SLP) was calculated by adding up ATP-producing fluxes and subtracting ATP-consuming fluxes in the carbon core network. ATP, synthesized from NADH, $FADH_2$ and $PQQH_2$ in the electron transport chain (ETC) via oxidative phosphorylation, was estimated considering a P/O ratio of 1.875 for NADH and $PQQH_2$ (Hardy et al., 1993; Oberhardt et al., 2011) and 1.0 for $FADH_2$ (Yuan et al., 2017). The anabolic ATP demand was calculated from the stoichiometric requirement for cellular synthesis, the biomass composition (van Duuren et al., 2013) and the observed specific growth rates (Table 2). In addition, ATP withdrawal for nongrowth-associated (NGA) maintenance was taken into account (van Duuren et al., 2013). Notably, strain MA-10 did not contain a flagellum. To reflect the absence of flagellum assembly and motion, a reduced cellular protein content (−1.0%) (Kerridge, 1959; McGroarty et al., 1973) and a lower energy expenditure (−2.1%) (Macnab, 1996) were considered when balancing MA-10.

2.12. Global gene expression profiling

For gene expression profiling, a custom-made microarray was designed and created (eArray, SurePrint G3, 8 × 60K, Agilent Technologies) using the recently revisited genome sequence of *P. putida* KT2440 (Belda et al., 2016). The microarray included three different 60-mer probes per gene plus internal controls. Total RNA of *P. putida* was isolated, cleaned up (RNeasy Mini Kit, Qiagen, Hilden, Germany, TURBO DNA-free Kit, Thermo Fisher Scientific, Waltham, MA, USA) and quantified (NanoDrop 1000, Peqlab Biotechnology, Erlangen, Germany). Subsequently, the RNA quality was assessed (RNA 6000 Nano Kit, 2100 Bioanalyzer System, Agilent Technologies). The RNA integrity number (RIN) of all samples was >8 as a criterion for sufficient quality. Fluorescence-labeled RNA was then prepared by direct chemical labeling of 50 ng native RNA (Low Input Quick Amp WT Labeling One-Color Kit, RNA Spike-In One-Color Kit, Agilent Technologies) according to the manufacturer's protocol. After cleaning and working up (RNeasy Mini Spin Columns, Agilent Technologies), the degree of labeling was measured (NanoDrop 1000, Peqlab, Erlangen, Germany). It was confirmed that at least 600 ng of labeled RNA with a specific activity of 15 (pmol Cy3) μg^{-1} was achieved for each sample. Subsequently, 600 ng labeled RNA was hybridized onto the microarray at 65 °C for 17 h in a dedicated hybridization chamber (Gene Expression Hybridization Kit, SureHyb chamber Agilent Technologies). Afterward, the hybridized slide was washed (Gene Expression Wash Buffer Kit, Agilent Technologies), transferred into the SureScan microarray scanner cassette (G2600D, Agilent Technologies), and scanned (SureScan Microarray Scanner G4900DA, Agilent Technologies) using the AgilentG3_GX_1-color scanner protocol with 3 μm double resolution. Data extraction and

processing was performed using microarray and feature extraction software (Version 12.1.1.1, Agilent Technologies). Transcriptomic data analysis and visualization were conducted using GeneSpring (Version 14.9, Agilent Technologies) and Bioconductor software (Gentleman et al., 2004). For statistical analysis, a moderated *t*-test was applied (Smyth, 2004), considering asymptotic computation of *p*-values adjusted for multiple testing according to the Benjamini-Hochberg method and a *q*-value cut-off of 0.05 (Benjamini and Hochberg, 1995). The data were then filtered for genes with a $\log_2$-fold change ≥ 1 (p value ≤ 0.05). RNA extraction and analysis were conducted in biological triplicates for each condition. The entire transcriptome data set is available at GEO (GSE196571).

2.13. Purification of biobased MA

A straightforward purification process was used to recover MA from the culture broth (Vardon et al., 2015, 2016). Following this strategy, biobased MA was purified from several batches of fermentation broth, obtained during this work (Kohlstedt et al., 2018). Hereby, the decolorization step was conducted twice. After removal of the activated carbon by filtration, MA was precipitated by acidification to pH 1.5 with 37% HCl. The, obtained crystals were washed once with deionized water and lyophilized (Christ, Osterode am Harz, Germany), which finally yielded a white crystalline powder.

2.14. Synthesis of the PET monomer bis (2-hydroxyethyl) terephthalic acid

A synthetic route from MA to bis (2-hydroxyethyl) terephthalic acid was developed, based on a previously patented strategy (Frost et al., 2013). During the development, identification and purity estimation of intermediates and products was carried out using UPLC (Agilent, Waldbronn, Germany) equipped with a C18 column (Acquity UPLC BEH C18, Waters, Eschborn, Germany) coupled to a diode array detector. Samples were dissolved in acetonitrile prior to analysis. In addition, intermediates and products were evaluated using ^{1}H-NMR (Avance III, 300 MHz, Bruker, Billerica, MA, USA) after dissolution in DSMO-d_6 or $CDCl_3$. Both analytical techniques were also used to monitor the reaction progress.

Isomerization of MA into *trans, trans*-muconic acid. First, MA was isomerized into *trans, trans*-muconic acid (TTMA, MW = 142.12 g mol^{-1}) using iodine (I_2) as a catalyst (Frost et al., 2013). For this purpose, MA and I_2 were dissolved in acetonitrile in a three-necked flask equipped with a reflux condenser, heated to reflux, and stirred under nitrogen (N_2). The reaction was monitored by ^{1}H-NMR for completeness. For product recovery, the resulting mixture was filtered hot, the retained solid was washed with acetonitrile, and the final, off-white crystals were dried under vacuum.

Esterification of *trans, trans*-muconic acid into the dimethyl ester. TTMA was suspended in methanol, treated with a catalytic amount of concentrated sulfuric acid and stirred at reflux, resulting in the formation of the corresponding dimethyl ester of TTMA (DMMA, MW = 170 g mol^{-1}). The reaction was monitored by ^{1}H-NMR. After completion, the reaction mixture was evaporated to dryness. The obtained solid was resuspended in methanol, filtered, and dried under vacuum.

Diels-Alder cyclization into 1,4-dimethyl cyclohex-2-ene-1,4-dicarboxylate. Third, DMMA was cyclized in a Parr reactor into 1,4-dimethyl cyclohex-2-ene-1,4-dicarboxylate (DMCD, MW = 198.2 g mol^{-1}) via a Diels-Alder reaction. For the conversion, DMMA was dissolved in *m*-xylene and saturated with ethylene (8 bar) as a dienophile. Subsequently, the mixture was heated to 200 °C, and the pressure reached 15 bar at this temperature. The reaction was monitored by ^{1}-H-NMR. After completion, the reaction mixture was concentrated under vacuum. The crude product was purified using preparative flash chromatography (Reveleris PREP, Grace, Columbia, MD, USA) with silica columns as the stationary phase (Chromabond Flash, 40 g silica, Macherey-Nagel) and cyclohexane/dichloromethane as the eluent. The obtained product was concentrated under vacuum. During development, other dienophiles, i.e., 1,2 dichloroethylene (Smith et al., 1980), trimethyl vinyloxy)silane (Müller and Miao, 1994), vinyl-pivalate (Lee et al., 1992), and ethyl vinyl ether (Juranovič et al., 2012), were tested as reaction partners at various concentrations and temperatures, as given below.

Oxidative aromatization into dimethyl terephthalic acid. Fourth, DMCD was oxidized into dimethyl terephthalic acid (DMTA, MW = 194.2 g mol^{-1}). The educt was dissolved in cyclohexane (0.1 M solution) in a Parr reactor, and 5% Pt/C (20 wt%) was added. The mixture was stirred at 150 °C under 8 bar air pressure and monitored using ^{1}H-NMR. After completion, the mixture was diluted with dichloromethane to dissolve the product that had precipitated at the bottom of the reaction vessel. Then, the obtained solution was filtered (Celite 545, Merck Millipore, Germany), and the filtrate was evaporated to dryness. The obtained crude product was purified by flash column chromatography (Chromabond Flash, 15 g silica, Macherey-Nagel) using cyclohexane/ethyl acetate as the eluent. Further stirring of the product-containing fraction in ice-cold pentane for 5 min yielded the desired DMTA at high purity. During development, other conditions were tested to attempt improved efficiency. These tests comprised the use of 2.2 equivalents of 2,3-dichloro-5,6-dicyanobenzoquinone as the oxidant with catalytic amounts of HCl, dioxane as solvent, and incubation at reflux (Brown and Turner, 1971); the use of 2.2 equivalents of 2,3-dichloro-5,6-dicyanobenzoquinone as the oxidant, toluene as the solvent, and incubation at reflux (Hilt and Danz, 2008); the use of 2.2 equivalents of chloranil as the oxidant, toluene as the solvent, and incubation at reflux; the use of Pt/C (4 mol% Pt) as the oxidant, acetic acid as the solvent, bubbling air, and incubation at 110 °C (Frost et al., 2010); and the use of 2.4 equivalents of benzoyl peroxide as the oxidant, dichloroethylene as the solvent, and incubation at 110 °C (Liu et al., 2017).

Transesterification into bis (2-hydroxyethyl) terephthalic acid. Four setups were evaluated to identify the optimum conditions for the base-catalyzed transesterification step. These setups comprised (i) the use of aqueous Na_2CO_3 as the base, ethylene glycol as the reagent, and acetonitrile as the solvent at 60 °C (Li and Lu, 2019); (ii) potassium *t*-butoxide as the base, ethylene glycol as the reagent, tetrahydrofuran as the solvent and a temperature of 60 °C (Cesati et al., 2015); (iii) NaOH as the base and ethylene glycol as the reagent/solvent at 80 °C (Koch and Götz, 2018); and (iv) *N,N*-diisopropylethylamine as the base and ethylene glycol as the reagent/solvent at 60 °C (Liu et al., 2017). The last strategy turned out to be most efficient. Therefore, DMTA was dissolved in ethylene glycol to 0.1 M. Subsequently, *N,N*-diisopropylethylamine (0.2 M) was added, the mixture was transferred into a two-necked flask, flushed with nitrogen, and heated to 60 °C to yield the transesterification product bis (2-hydroxyethyl) terephthalate (BHET, MW = 254.2 g mol^{-1}). The reaction was monitored by UPLC. After completion, the obtained reaction mixture was diluted with 100 mL of ultra-pure water and extracted with dichloromethane (4 × 200 mL). The organic phase was dried over $MgSO_4$ and concentrated under vacuum. The crude product was purified to a white crystalline solid by flash column chromatography (Chromabond Flash, 15 g silica, Macherey-Nagel) using dichloromethane/methanol as the eluent.

2.15. Polymerization of bis (2-hydroxyethyl) terephthalic acid into PET

BHET (1.2 g), together with 38 mg of antimony oxide (Sb_2O_3), was transferred into a microwave vial (Reining et al., 2002). The vial was sealed, submerged in a preheated oil bath (220 °C), and put under vacuum (20 mbar). After boiling and melting of the mixture, PET started forming and precipitating, and a solid polymer block was obtained. After cooling to room temperature, the solid was crushed and suspended in MeOH. The liquid was decanted off, and the solid PET polymer was dried

under vacuum. Thermal analysis of the final polymer's melting temperature was carried out on a thermogravimetric analyzer (Linseis, Selb, Germany).

3. Results

3.1. The growth and MA production capacity of P. putida KT2440 strains are strongly inhibited by catechol

A centerpiece of the envisioned value chain was to efficiently convert the lignin-based aromatic catechol into MA. Industrially, catechol is frequently obtained during lignin depolymerization (Schutyser et al., 2018). Metabolically, catechol is the terminal pathway intermediate of MA biosynthesis and is therefore involved in the conversion of every lignin monomer into this product (Nogales et al., 2017), which poses a risk of accumulation, specifically during the use of crude aromatic mixtures (Weiland et al., 2021). As a starting point for quantitative evaluation, the tolerance of wild-type *P. putida* KT2440 toward catechol was assessed in a small-scale cultivation system during growth on glucose. Here, the chosen setup mimicked MA production from aromatics that required a second growth substrate, typically glucose, due to a disruption of the β-ketoadipate pathway (Kohlstedt et al., 2018). Under these conditions, catechol was found to be strongly inhibitory (Fig. S1, supplementary file 1). Even low catechol levels led to extended lag phases and reduced specific growth rates, and growth of the cells was completely abolished at 8.0 mM of the aromatic. Next, we analyzed the KT2440-based MA producer *P. putida* MA-1, which lacked the *catBC* genes to prevent further conversion of MA in the catechol branch of the β-ketoadipate pathway. The MA-1 mutant was as sensitive as the wild type, and growth was also arrested at a catechol concentration of 8.0 mM (Fig. 1). The half-maximal inhibitory concentration ($IC_{50,\ catechol}$), a widely used measure for toxicity, was reached at 6.3 mM.

In shake flask-based production experiments using 5 mM catechol together with 30 mM glucose as the growth substrate, the catechol susceptibility of strain MA-1 caused (again) an extensive lag phase. Significant conversion of catechol to MA started after 45 h (Fig. 2A). MA was stoichiometrically formed (5 mM). In its inhibited state, strain MA-1 required 52 h to fully metabolize glucose. Gluconate and, to a lesser extent, 2-ketogluconate accumulated as byproducts, indicating incomplete catabolization of glucose due to periplasmic oxidation (Nikel et al., 2015). Later, the two organic acids were again taken up by the cells,

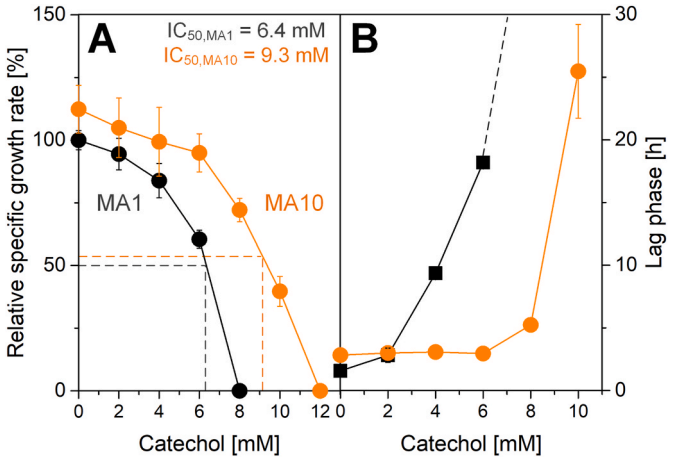

Fig. 1. Impact of catechol on the growth of the *cis, cis*-muconate-producing strains *Pseudomonas putida* KT2440 MA-1 and MA-10. The aromatic was added at different levels to the glucose-based minimal medium. Growth was monitored online and yielded the specific growth rate (A) and the lag phase (B) for each condition. For each strain, the data are normalized to growth without catechol as a reference (Table 2). The corresponding data for the KT2440 wild type is shown in Fig. S1 (supplementary file 1). n = 2.

resulting in co-consumption together with the remaining glucose. Altogether, catechol intoxication appeared as a great challenge to the fermentative conversion of technical lignin streams using *P. putida* KT2440.

3.2. Under catechol stress, P. putida MA-1 shifts from periplasmic to cytoplasmic glucose metabolism and enhances the TCA cycle flux

Next, we studied the catechol effects in more detail on the metabolic level to eventually discover targets for strain optimization. *P. putida* KT2440 operates a cyclic metabolism, the so called EDEMP cycle, which merges activities belonging to the EMP, the ED, and the PP pathways into a complex architecture (Nikel et al., 2015). This network comprises three parallel routes for glucose catabolism after uptake of the sugar into the periplasm (del Castillo et al., 2007). The routes activate the substrate at the level of either glucose, gluconate or 2-ketogluconate, respectively, before they merge at the central intermediate 6-phosphogluconate (Fig. 3A). In the following, we name them glucose (phosphorylating), gluconate (phosphorylating), and 2-ketogluconate (phosphorylating) pathways. The glucose-phosphorylating route supplies redox power at elevated energy costs (Fig. 3B). The gluconate-phosphorylating route is redox-neutral, whereas the 2-ketogluconate-phosphorylating route consumes redox power at increased energy supply. The differences in energy and redox stoichiometry offer flexibility to respond to specific demands and environments (Kohlstedt and Wittmann, 2019).

To elucidate the catechol effects in more detail, we studied strain MA-1 by ^{13}C metabolic flux analysis and determined the intracellular flux distributions of the glucose-grown microbe in the presence of 5 mM catechol and without catechol (reference). For both conditions, parallel tracer cultures on [1–^{13}C], [6–^{13}C], and 50% [$^{13}C_6$] glucose were conducted, and cells were analyzed for the labeling patterns of amino acids, glucose, and glucosamine, yielding 534 mass isotopomers for high-resolution flux analysis. In both cases, the estimation revealed an excellent fit of the labeling data and a high precision of the obtained fluxes (Table S3, supplementary file 1). When grown on glucose alone, strain MA-1 revealed a split use of the sugar (Fig. 3C). The microbe processed more glucose via the (2-keto)gluconate phosphorylating routes (61%) than the glucose-phosphorylating route (39%), favoring the formation of ATP (Fig. 3AB). The periplasmic intermediates gluconate and 2-ketogluconate were largely converted into 6-phosphogluconate (56%), whereas only small fractions were secreted. Furthermore, 6-phosphogluconate was almost exclusively converted via the ED pathway (115%), providing pyruvate and glyceraldehyde 3-phosphate at high flux, whereas the oxidative PP pathway was practically inactive (1%). More than half of the formed glyceraldehyde 3-phosphate (63%) was recycled back to hexose phosphates, supporting formation of NADPH by glucose 6-phosphate dehydrogenase (60%). Additional NADPH was supplied by malic enzyme (53%) and isocitrate dehydrogenase (82%). Overall, glucose-grown MA-1 resembled the flux distribution of the KT2440 wild type, previously studied on glucose, in all relevant features (Kohlstedt and Wittmann, 2019; Kukurugya et al., 2019).

When grown in the presence catechol, MA-1 revealed a strongly changed flux distribution (Fig. 3D). Stressed by the aromatic, cells shifted flux from the (2-keto)gluconate-phosphorylating routes to the glucose-phosphorylating route. Periplasmic glucose oxidation was reduced from 61 to 48%, while the transport flux of glucose into the cytosol was increased from 39 to 52%. Based on stoichiometry, this flux shift increased NADPH generation at additional ATP costs (Fig. 3AB). The oxidative PP pathway was still inactive so that the cells could not generate NADPH via this route. However, the pyruvate shunt was activated instead. The flux through malic enzyme (involved in the shunt) was slightly higher (64 versus 53%), generating more NADPH. At the same time, MA-1 burned more carbon in the TCA cycle. The TCA cycle flux was approximately 1.2-fold higher than that in the control culture. The relative amount of CO_2 formed under catechol stress (302%) was

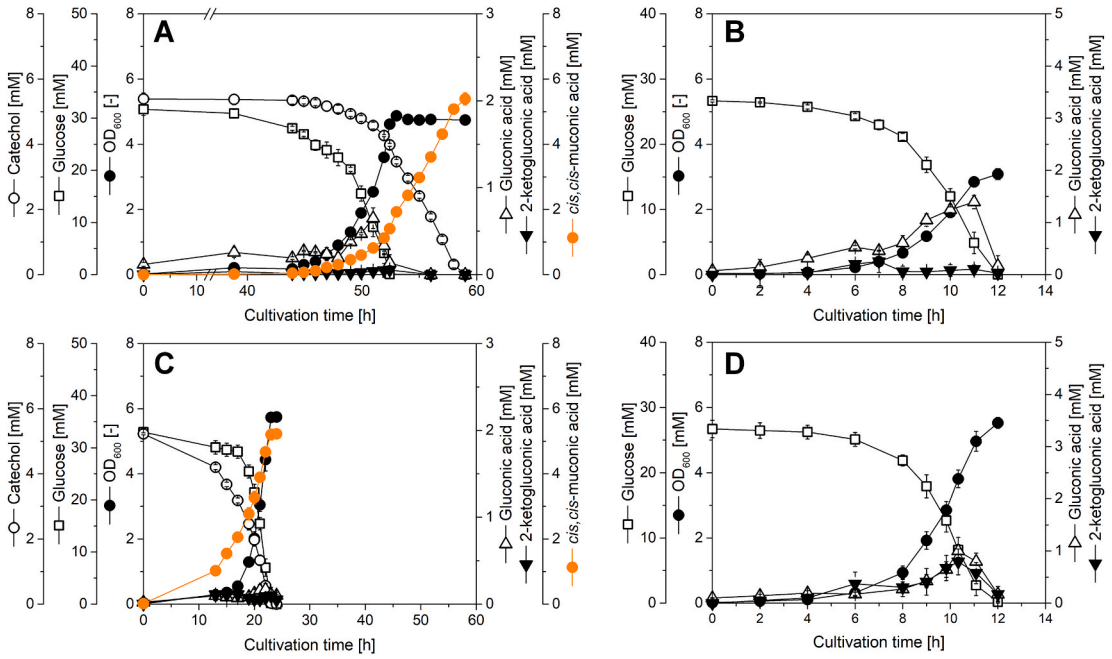

Fig. 2. Growth and *cis, cis*-muconate production of *Pseudomonas putida* KT2440 MA-1 and MA-10. The two strains MA-1 (A, B) and MA-10 (C, D) were studied in shake flask cultures. First, growth and MA production from 10 mM glucose (as a growth substrate) and 5 mM catechol (as an MA precursor) were assessed (A, C). Second, both strains were studied during growth on glucose alone (B, D). The data comprise growth of the cells, consumption of glucose and catechol, and formation of MA, gluconate, and 2-ketogluconate. n = 3.

substantially higher than that of the control (250%). This finding was consistent with the lower biomass yield of stressed cells (Table 2). Notably, the 20% reduced specific glucose uptake rate under catechol stress superimposed the relative flux changes. As an example, the relative flux increase, observed for the glucose-phosphorylating route and the TCA cycle (Fig. 3CD) maintained the absolute flux rate through these pathways under stress inhibited (Table S5, supplementary file 1). The reduction of the glucose uptake rate, caused by catechol, differed from the sometimes-observed enhanced glucose uptake observed in the presence of organic solvents, such as toluene or styrene (Blank et al., 2008).

3.3. Transcriptional control superimposes the rerouting of intracellular fluxes and involves changes in isoenzyme expression at important branch points

Approximately 28% of all genes were significantly changed in expression when strain MA-1 was challenged with catechol (supplementary file 2, log2-fold change $\geq$1, p $\leq$ 0.05). While 913 genes were upregulated, 686 genes were downregulated. The transcriptional response included the upregulation of genes involved in the oxidative stress response and cellular repair processes, as typically observed for microbes under catechol stress (Tam et al., 2006). Several changes were related to carbon core metabolism, likely contributing to the observed flux changes (Fig. 4, Table S6, supplementary file 1). First, the two catabolic operons *kgu* and *gad,* encoding periplasmic gluconate metabolism and usually induced during growth on glucose, gluconate, and 2-ketogluconate (del Castillo et al., 2007), were strongly repressed. Both operons are under the control of *ptxS*, which also controls its own synthesis (Daddaoua et al., 2010), and this regulator was likewise downregulated. Second, the expression of ZwfA and ZwfB, which differ in their kinetic behavior (Volke et al., 2021), was downregulated and upregulated, respectively. Isoenzyme changes were further found for the TCA cycle, including *acnA* (up) and *acnB* (down), as well as *mdh* (up), *mqo2* (up), *and mqo3* (down). Third, catechol stress affected the expression of genes associated with the respiratory chain, ATP synthesis, and the (energy consuming) flagellum, as previously observed in *P. putida* under oxidative stress (Hallsworth et al., 2003). The membrane-bound transhydrogenase PntAB was upregulated, correlating to observations that transhydrogenases play a role in redox balancing when bacteria face aromatic carbon sources, as exemplified for *P. putida* (Nikel et al., 2016), *Sphingobium* sp. SYK-6 (Varman et al., 2016), and *R. opacus* (Roell et al., 2019). Taken together, MA-producing *P. putida* MA-1 exhibited transcriptional changes that accompanied the shift in intracellular fluxes under prolonged catechol stress. In this regard, the immediate flux response of *P. putida* to sublethal doses of diamide as a proxy of oxidative stress (Nikel et al., 2021), together with our data, reveal interesting differences between short- and long-term responses of the microbe to oxidative stress.

3.4. Catechol-stressed P. putida MA-1 exhibits an increased NADPH availability for stress defense

Catechol detoxification in microbes requires substantial amounts of redox power and energy (Schweigert et al., 2001). To provide a quantitative picture for the studied microbe, we balanced the supply and demand for redox power (NADPH) and energy (NADH, $PQQH_2$, $FADH_2$, ATP) (Fig. 5). MA-1 supplied 13.1 mmol g^{-1} h^{-1} NADPH, mainly used for anabolic purposes (Fig. 5A), a range that matched well with that of the glucose-grown wild type (Nikel et al., 2015). Overall, an apparent excess of NADPH was available to the microbe, as also observed in other microbes (Becker et al., 2005; Wittmann and Heinzle, 2002; Wittmann et al., 2004). Under catechol stress, the absolute NADPH supply was maintained (12.9 mmol g^{-1} h^{-1}), although 20% less glucose was taken up. The reduced biomass yield (and the consequently lower anabolic NADPH requirement) increased the apparent surplus (for stress defense) by 36%. This flux change nicely matched with the fact that NADPH displays the central redox metabolite that fuels the oxidative stress response in *P. putida* (Bitzenhofer et al., 2021) and related pseudomonads (Singh et al., 2007), and its balanced supply is important to confer stress tolerance (Akkaya et al., 2018). Catechol, however, lowered the ATP supply by (at least and probably more than) 10% (Fig. 5C). Despite the lowered anabolic ATP demand, the cells did not increase the apparent ATP excess for stress defense. This phenomenon could explain

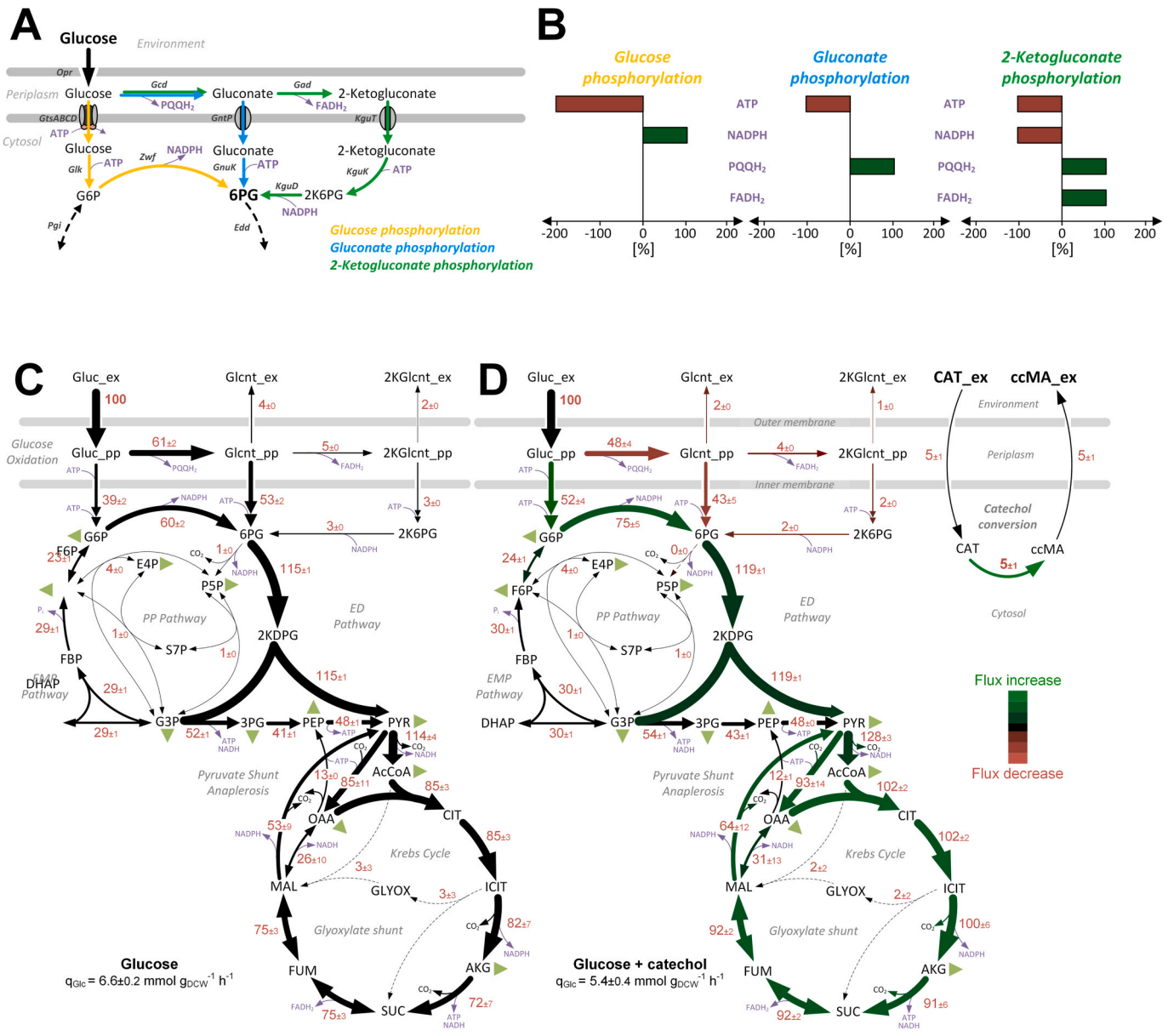

Fig. 3. Carbon core metabolism of *cis, cis*-muconate-producing *Pseudomonas putida* KT2440 MA-1. Parallel routes for glucose catabolism and associated energy and redox stoichiometry (A, B), and impact of catechol on intracellular carbon fluxes determined by ^{13}C metabolic flux analysis (C, D). Regarding network structure, glucose enters the periplasmic space through specific OprB porins and it is then internalized into the cytoplasm or oxidized to gluconate and/or 2-ketogluconate in the periplasm, resulting in three parallel routes that finally merge at the 6-phosphogluconate node: (i) the glucose phosphorylating route with oxidation of glucose into the cytoplasm by an ABC transporter, phosphorylation and subsequent oxidation (del Castillo et al., 2007), (ii) the gluconate-phosphorylating route with proton-coupled gluconate transport into the cytosol and phosphorylation (Bator et al., 2020), (iii) the 2-ketogluconate-phosphorylating route with periplasmic gluconate oxidation to 2-ketogluconate, which is then transported (driven by sodium) into the cytoplasm, phosphorylated, and reduced to 6-phosphogluconate. $PQQH_2$ and $FADH_2$ are channeled into the electron transport chain and contribute to ATP formation (Ebert et al., 2011), whereby P/O ratios of 1.875 for $PQQH_2$ (Hardy et al., 1993; Oberhardt et al., 2011) and 1.0 for $FADH_2$ (Yuan et al., 2017) have been proposed. Regarding ^{13}C metabolic flux analysis, strain MA-1 was studied during growth on glucose (C) and during growth on glucose plus 5 mM catechol (D). For each condition, the fluxes are given as a molar percentage of the corresponding specific glucose uptake rate of $q_{Glc} = 6.6$ mmol g^{-1} h^{-1} (C) and $q_{Glc} = 5.4$ mmol g^{-1} h^{-1} (D), which was set to 100%. The reactions generating biomass are indicated as green triangles. Their flux values can be taken from Table S2. The *in vitro* activity of GnuK and KguK was found to be similar for both conditions, and the resulting GnuK/KguK activity ratio of 20:1 was used to constrain the flux split at the gluconate node. During flux estimation, an excellent fit of the ^{13}C data was obtained (Table S3, supplementary file 1). n = 3.

why the strain previously exhibited a depleted adenylate energy charge during prolonged MA production from lignin-related aromatics (Kohlstedt et al., 2018). It should be noted, however, that the data do not provide a causality, in weather the observed changes in energy and redox metabolism were actively mediated or indirectly resulted from the stress at reduced glucose influx.

3.5. *The genome-reduced cell factory P. putida MA-10 reveals superior catechol tolerance and MA production in shake flask cultures*

Inspired by the potential of an energetically improved metabolism, we established MA production in *P. putida* EM42, a genome-reduced derivative of KT2440 with improved growth properties and physiological vigor (Martinez-Garcia et al., 2014). First, we mirrored the basic producer *P. putida* MA-1 by deleting muconate cycloisomerase (catB)

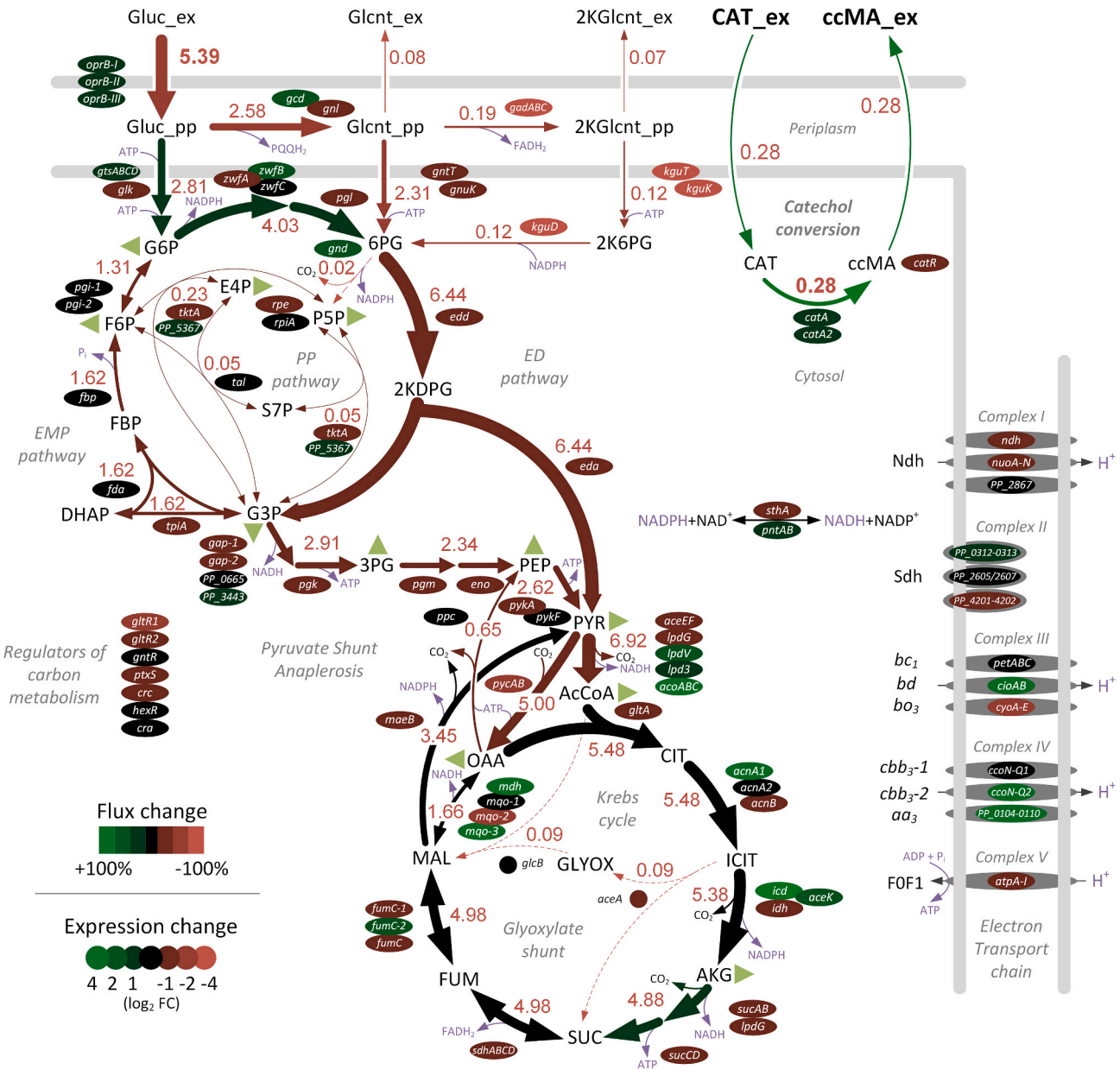

Fig. 4. Integrated view of the metabolic and transcriptional response of the carbon core metabolism of *Pseudomonas putida* KT2440 MA-1 to catechol stress. The data comprise changes in absolute carbon fluxes determined by ^{13}C metabolic flux analysis and inferred from the relative fluxes (Fig. 3CD) and the specific glucose uptake rate of $q_{Glc} = 5.4$ mmol g^{-1} h^{-1} (Table 2). On top, the expression levels of the encoding genes are shown as log_2-fold changes. When multiple isoforms exist for a given enzyme, they are represented separately, and the individual isoenzyme names are specified. For enzyme complexes, the given expression level represents the averaged value of the individual subunits. The statistical quality of the transcriptome data was verified by PCA (Fig. S2, supplementary file 1). n = 3.

and muconolactone Δ-isomerase (catC) (Kohlstedt et al., 2018) in EM42. The corresponding mutant, verified for the desired deletions by PCR and sequencing, was designated *P. putida* MA-10. On glucose, it showed the same growth properties as EM42. Additionally, it formed MA from catechol and benzoate at stoichiometric yield, using glucose as a growth substrate (Table 2). Furthermore, MA-10 revealed substantially improved tolerance and could grow at catechol levels above 10 mM (Fig. 1). At this high concentration, growth of MA-1 was impossible. In quantitative terms, the inhibition constant of the genome-reduced producer ($IC_{50,\ CAT} = 9.3$ mM) was almost 50% higher than that of MA-1. Furthermore, MA-10 was found to be superior for catechol-based MA production in shake flasks, using glucose as a growth substrate. The mutant exhibited a significantly reduced lag phase and produced MA almost three times faster than MA-1 (Fig. 2C). Hereby, MA-10 achieved a 60% higher cell concentration. The increased biomass yield provided more biocatalytic cells, contributing to the superior performance (Table 2). A higher biomass yield for MA-10 was also observed when both mutants were grown on glucose alone (Fig. 2 BD). Overall, the improved stress tolerance displayed a promising feature toward process applicability (Jayakody et al., 2018).

3.6. *The flux distribution of strain MA-10 is optimized for increased carbon efficiency at reduced energy and redox metabolism*

MA-10 was now also studied using ^{13}C metabolic flux analysis. It catabolized glucose mainly via the (2-keto)gluconate-phosphorylating routes (Fig. 6A). Compared to its wild-type-based counterpart MA-1, periplasmic glucose oxidation was even increased in flux (80% versus

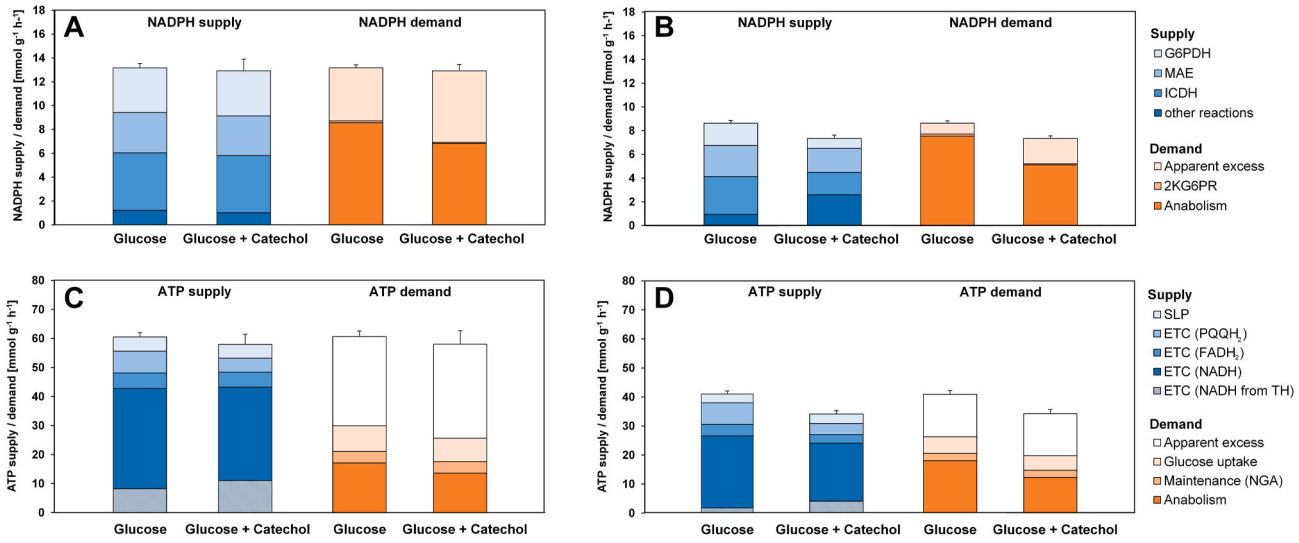

Fig. 5. Impact of catechol on redox and energy metabolism in *Pseudomonas putida* KT2440 MA-1 and MA-10. The data represent absolute balances for NADPH in MA-1 (A) and MA-10 (B) and absolute balances for energy in MA-1 (C) and MA-10 (D), inferred from the obtained intracellular flux distributions, considering enzymatic cofactor specificity. Notably, millimolar concentrations of catechol are known to uncouple electron transport from ATP synthesis and to destroy the membrane potential by perturbation of the lipid bilayer (Schweigert et al., 2001), affecting the energy efficiency of the ETC. In this light, the total ATP supply under catechol stress, calculated here by assuming the P/O ratio of unstressed cells, reflected an optimum scenario. It cannot be excluded that less ATP was generated in reality than in theory. Abbreviations: G6PDH, glucose 6-phosphate dehydrogenase; MAE, malic enzyme; ICDH, isocitrate dehydrogenase; 2KG6PR, 2-ketogluconate 6-phosphate reductase; SLP, substrate level phosphorylation; ETC, electron transport chain; NGA, nongrowth-associated.

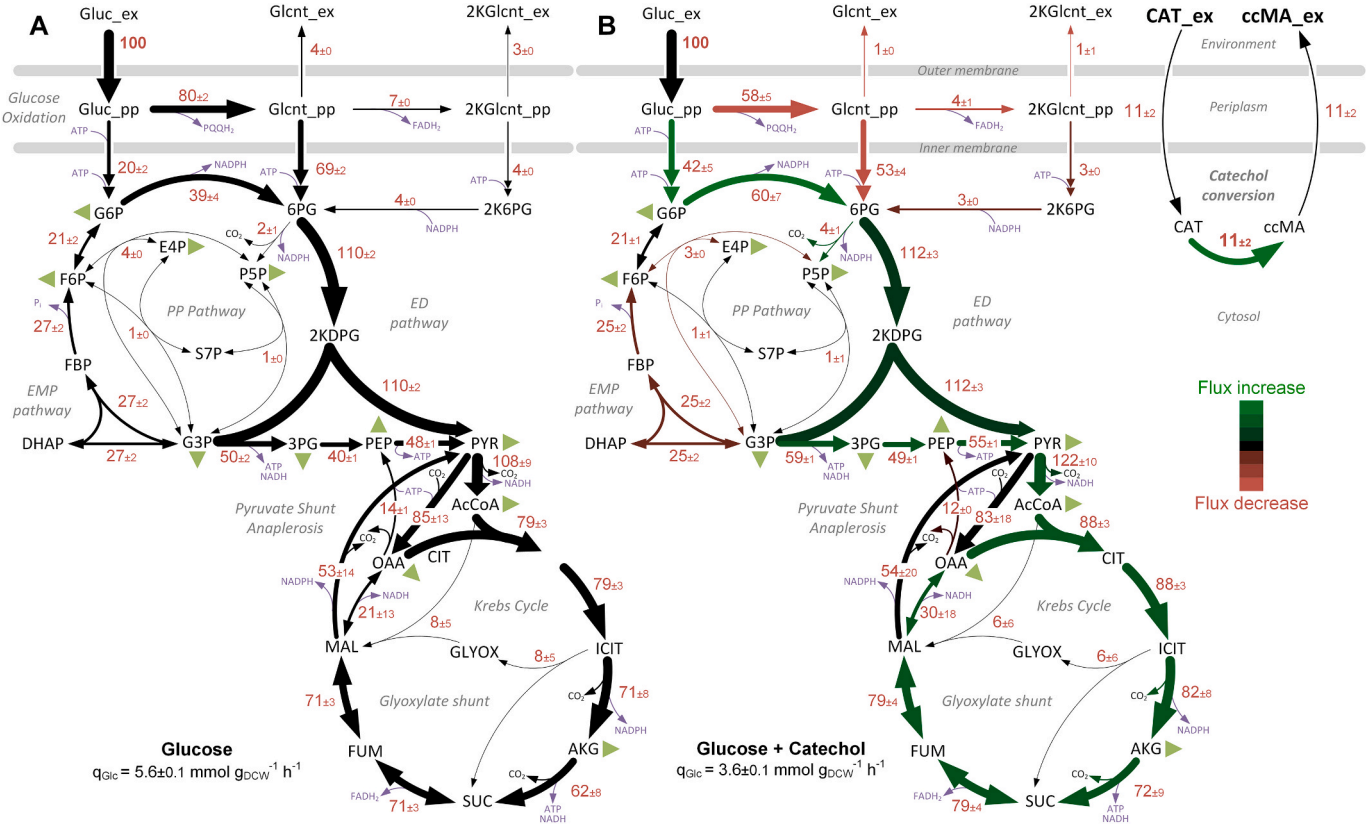

Fig. 6. Impact of catechol on intracellular carbon fluxes of the advanced *cis, cis*-muconate-producer *Pseudomonas putida* KT2440 MA-10 determined by ^{13}C metabolic flux analysis. The strain was studied during growth on glucose (A) and during growth on glucose plus 5 mM catechol (B). For each condition, the fluxes are given as a molar percentage of the corresponding specific glucose uptake rate of $q_{Glc} = 6.6$ mmol g^{-1} h^{-1} (A) and $q_{Glc} = 5.4$ mmol g^{-1} h^{-1} (B), which was set to 100%. The reactions generating biomass are indicated as green triangles. Their flux values are not shown here but can be taken from Table S2. The *in vitro* activity of GnuK and KguK was found to be similar for both conditions, and the resulting GnuK/KguK activity ratio of 20:1 was used to constrain the flux split at the gluconate node. During flux estimation, an excellent fit of the ^{13}C data was obtained (Table S4, supplementary file 1). n = 3.

61%), whereas the flux through the (energy-costly) glucose-phosphorylating pathway was only half as high (20% versus 39%). Interestingly, the TCA cycle flux was reduced in MA-10 and, altogether, less carbon was released as CO_2 (225%). In summary, MA-10 provided substantially less redox power and energy. The total supply of ATP (39.2 mmol g^{-1} h^{-1}) and NADPH (8.6 mmol g^{-1} h^{-1}) was 25% and 34% lower than that in the wild-type-based strain, respectively (Fig. 5BD). While looking less efficient at first glance, MA-10 used less glucose, as inferred from the 20% reduced specific uptake rate. Furthermore, MA-10 generated much more biomass (Table 2). Notably, the apparent surplus of ATP and NADPH was significantly lower in MA-10. This observation might be explained by the partial elimination of redox- and energy-demanding processes (which would have otherwise accounted for the use of the apparent surplus) resulting from elimination of the flagellum and other changes (Martinez-Garcia et al., 2014). In this regard, the MA-10 mutant responded to the lowered energy and redox requirement by reducing supply and used the extra carbon (not lost in decarboxylation) for growth at increased yield, reflecting the principle of metabolism driven by demand (Tiso et al., 2016).

When challenged with catechol, MA-10 revealed a number of flux adaptations (Fig. 6B). Qualitatively, many of them matched the flux response by MA-1. Carbon flux was shifted from the (2-keto)gluconate-phosphorylating to the glucose-phosphorylating pathways, boosting NADPH formation at additional ATP expense, while the activity of the TCA cycle was enhanced. However, the flux changes differed strongly from that of MA-1 in quantitative terms. The flux redirection at the periplasmic glucose node was much stronger, while the flux increase through the TCA cycle was less pronounced. In contrast to MA-1, malic enzyme was not activated. Interestingly, strain MA-10 converted catechol into MA more than twice as fast as MA-1 when normalized to glucose uptake (Figs. 3B and 6B). In addition, MA-10 increased its apparent NADPH excess under catechol stress 2.4-fold, significantly more than MA-1 (1.8-fold) (Fig. 5).

3.7. The genome-reduced EM42 chassis offers increased robustness to different lignin monomers, including cinnamates and phenolics

Next, we evaluated the tolerance of the novel genome-reduced derivative to a wider range of cinnamates, aromatic acids, and alcohols, which were assumed to be relevant for lignin upgrading based on previous studies (Barton et al., 2018; Rodriguez et al., 2017; Toledano et al., 2012). Compared to the wild type, the genome-reduced chassis EM42 provided increased robustness to withstand a range of structurally variable lignin-associated aromatic compounds (Fig. 7). EM42 grew faster in the presence of elevated levels of caffeate and *p*-coumarate (and to some extent vanillate) than KT2440. Exemplified for *p*-coumarate and vanillate, the tolerance of the latter well matched with previous work (Salvachua et al., 2018). EM42 revealed shorter lag phases when higher amounts of caffeate, *p*-coumarate, vanillate, benzoate, and phenol were added. Phenol was found to be almost as toxic as catechol and enabled growth only up to a level of 15 mM. Notably, for differently substituted aromatic carboxylic acids, such as the vanillate, benzoate and protocatechuate, elevated concentrations were tolerated. The overall better performance of strain EM42 appears attractive. Catechol and phenol are prominent examples of (typically rather toxic) technical lignin monomers that emerge from harsh depolymerization methods (van Duuren et al., 2020), often necessary for efficient depolymerization of highly compacted lignins of industrial waste streams (Weiland et al., 2021), whereas *p*-coumarate, ferulate and vanillate are majorly found in lignin hydrolysates from base-catalyzed depolymerization from corn-stover lignin (Rodriguez et al., 2017). Therefore, the broadly increased robustness of strain EM42 suggests promising potential for the valorization of different lignin streams (Weiland et al., 2021). Surprisingly, EM42 was more sensitive to guaiacol than the wild type, requiring more work to identify (and eventually stream-line) the capability of genome-reduced derivatives for lignin valorization.

3.8. *P. putida* MA-10 accumulates 74 g L^{-1} MA from catechol and outcompetes the wild-type-based counterpart MA-6 in productivity and titer

Next, we benchmarked the strains MA-1 and MA-10 for their MA production performance under industrially relevant conditions. First, we tested them in a fed-batch process that challenged the cells with inhibitory shots of catechol towards high MA titer (in short time) and, consequently, high productivity (Fig. 8A, B, C, D). After less than 10 h, the initially supplied sugar (7.5 g L^{-1}) was depleted by both producers, and the feed phase was started, including 5 mM catechol pulses and exponential feeding of glucose as a growth substrate. During the first 33 h, both strains performed similarly well. Up to this point, they reached maximum optical densities of 23.7 (MA-1) and 25.2 (MA-10) and accumulated MA to titers of 44.4 g L^{-1} (MA-1) and 45.2 g L^{-1} (MA-10), while the catechol and glucose levels remained low. Then, MA-10 started to outperform (Fig. 8B). While growth stopped, the level of MA increased steadily and reached a final titer of 73.8 g L^{-1} after 90 h. A small amount of glucose that transiently accumulated was completely taken up again later. Interestingly, a large fraction of the sugar was oxidized into 2-ketogluconate during this late process stage, 90.2% on a

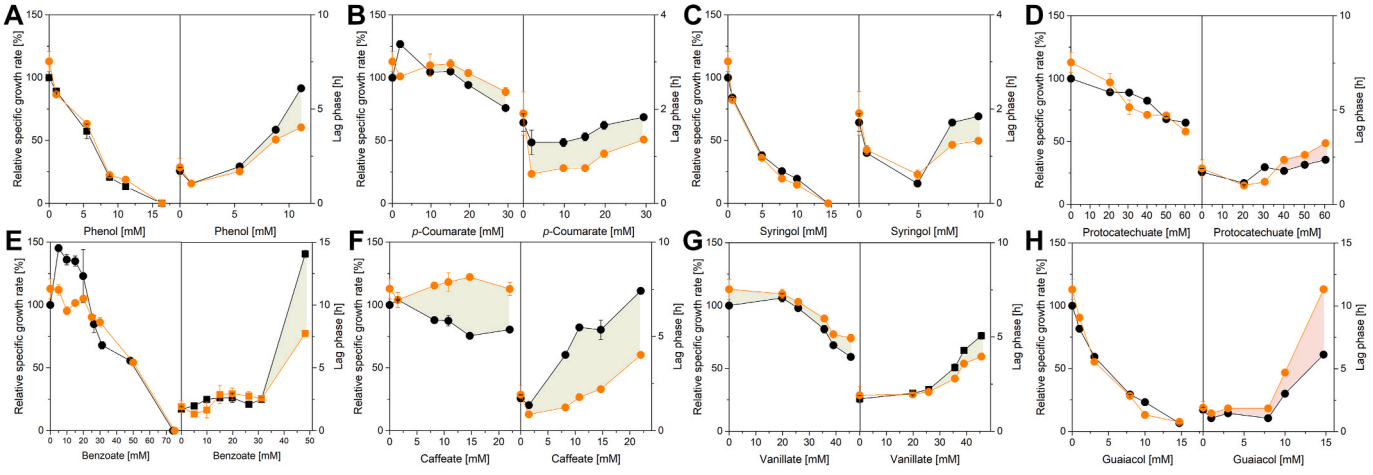

Fig. 7. Impact of eight lignin-based aromatics on the growth of *P. putida* KT2440 MA-1 and its genome-reduced counterpart EM42. Each aromatic was added at different levels to the glucose-based minimal medium. Growth was monitored online and yielded the specific growth rate and the lag phase for each condition. For each strain, the data are normalized to growth without the aromatic as a reference (Table 2). n = 2.

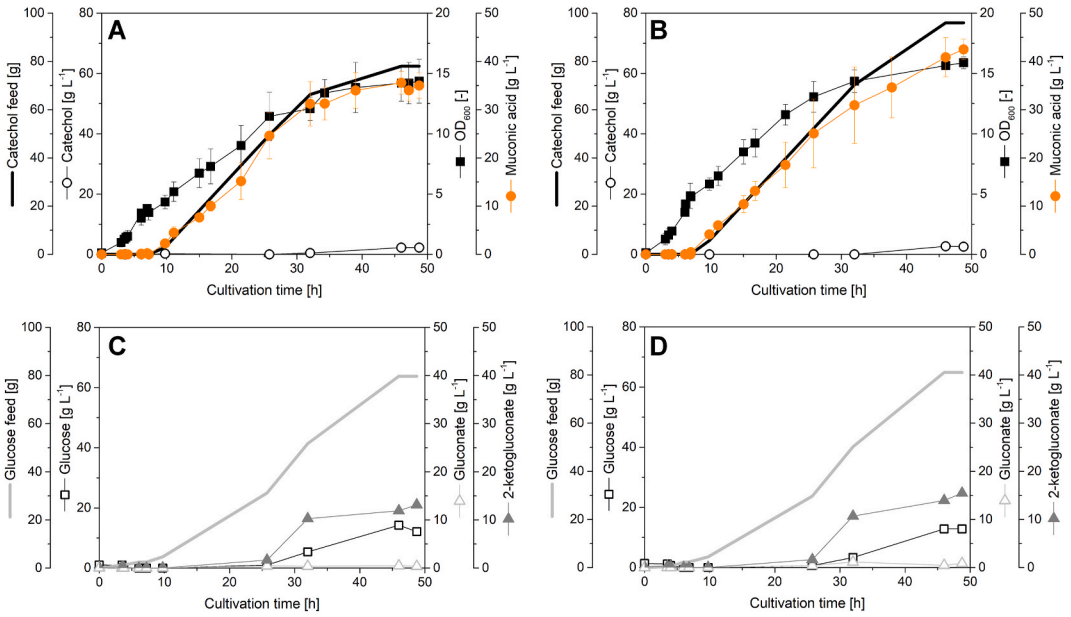

Fig. 8. Rate-optimized fed-batch production of *cis, cis*-muconate by metabolically engineered *Pseudomonas putida* MA-1 (A, C) and MA-10 (B, D). After depletion of the initial glucose at the end of the batch phase, the sugar was fed exponentially. Catechol pulses (5 mM) were added automatically, using a sudden increase in the dissolved oxygen level as a trigger. Deviations for this type of fermentation are in the range of 5% (Kohlstedt et al., 2018) (see also Fig. 9).

molar basis (Fig. 8D). The maximum space-time yield (1.4 g L^{-1} h^{-1}) for MA-10 was obtained after 44 h. On average, MA was formed at a space-time-yield of 1.2 g L^{1} h^{-1}, more than 80% of the maximum value, indicating a robust process. In comparison, MA-1 formed only 61.6 g L^{-1} MA, whereby formation of the product was restricted to the first 60 h of fermentation (Fig. 8A). Notably, the mutant accumulated catechol after this time point. Glucose, fed into the reactor, now largely accumulated. A certain fraction of the added sugar was, however, still metabolized and ended up at almost 100% in 2-ketogluconate (Fig. 8C). The maximum and the average space-time yield of strain MA-1 (1.3 and 1.1 g L^{-1} h^{-1}) were 15% lower than the values for strain MA-10.

Overall, the energy-optimized strain MA-10 was found to be superior. Particularly in later stages of the process, when microbial cell factories typically start to suffer (Giesselmann et al., 2019; Hoffmann et al., 2021; Rohles et al., 2018), the MA-10 mutant remains productive. Interestingly, *P. putida* exhibited a novel mode of metabolism during the second half of the fed-batch process: conversion of catechol into MA at zero growth with extensive periplasmic glucose oxidation to form energy. To some extent, this mode relates to the metabolic behavior of *P. putida* in anoxic electro fermentation, where cells do not grow but oxidize 90% of glucose into 2-ketogluconate (Lai et al., 2016). The MA titer, achieved with MA-10, sets a new benchmark among aromatic-based production processes (Weiland et al., 2021; Xie et al., 2014) and, considering recent life cycle and cost assessment (Corona et al., 2018; van Duuren et al., 2020), brings the valorization of lignin for the manufacturing of this commercially recognized chemical one step further to industrialization.

3.9. The advanced producer P. putida MA-11 enables MA production from catechol at a 30% reduced glucose requirement in a yield-oriented, fed-batch system

Next, we wanted to see if more advanced MA producers could also benefit from a streamlined carbon core metabolism. We created strain MA-11 on the basis of *P. putida* MA-6, a recently developed strain that exhibited enhanced robustness to catechol ($IC_{50,\ Catechol}$ = 8.3 mM) and improved MA production performance due to genomic expression of a catechol control and conversion (CCC) element (Kohlstedt et al., 2018). In summary, we installed the synthetic CCC module of MA-6 in the genome-reduced strain MA-10 and thereby expressed a second catechol 1,2-dioxygenase gene (*catA2*) under the control of the native P_{cat} promoter (Kohlstedt et al., 2018). Strain MA-11 was verified for the correctness of the desired genomic changes by PCR and sequencing.

To benchmark MA-6 and MA-11, we selected a yield-oriented process configuration (Fig. 9). To this end, we batched glucose at a low level (1.8 g L^{-1}) at the process start and, after depletion, fed the sugar to both strains at the same rate. Catechol was automatically added in pulses using the pH value as an online signal. Each catechol pulse was chosen to be small so that the aromatic level remained below 0.5 mM to cause presumably no or at least only weak inhibition. Both strains started to grow immediately and performed relatively similarly during the batch phase. Glucose was consumed within 6 h, and the same cell concentration was reached. Then, MA-11 handled the shift to limited feeding better, while MA-6 was shortly halted in growth. Furthermore, MA-11 maintained a slight growth advantage and exhibited a 15% higher cell concentration than MA-6. Both strains, however, did not differ in production performance. After 26 h, MA-6 (24.5 g L^{-1}) and MA-11 (25.1 g L^{-1}) achieved almost the same MA titer. The fact that the speed of catechol addition was controlled by the cells themselves indicated that both chassis, wild-type-based and genome-reduced, provided the same performance at this early point of the process. Then, the metabolism of the cells obviously changed, and they similarly started to accumulate glucose, 2-ketogluconate and finally catechol. During the second half of the fermentation, MA-11 performed much better: it continued to synthetize more product and reached a final MA titer of 44.1 g L^{-1} after 48 h, i.e., accumulated almost 20 g L^{-1} extra product toward the end of the process. In contrast, MA-6 slowed down production. Its final MA level (35.2 g L^{-1}) was 25% lower than that of MA-11. Moreover, MA-11 was found to have a much better sugar utilization efficiency. Overall, both strains received the same amount of glucose (165 mmol), but MA-11 converted significantly more catechol during the same time (205 versus 165 mmol in MA-6). In terms of glucose use relative to produced MA, MA-11 (1.38 ± 0.10 mol (mol glucose)$^{-1}$) surpassed MA-6 (1.02 ± 0.02 mol (mol glucose)$^{-1}$) by 35%. Even though promising attempts aim to replace the commonly used glucose by less expensive substrates (Johnson et al., 2017; Sonoki et al., 2018; Zhang et al., 2015), the need for additional carbon reduces the overall performance, and a more economic use of the growth substrate is desirable. In this regard, the

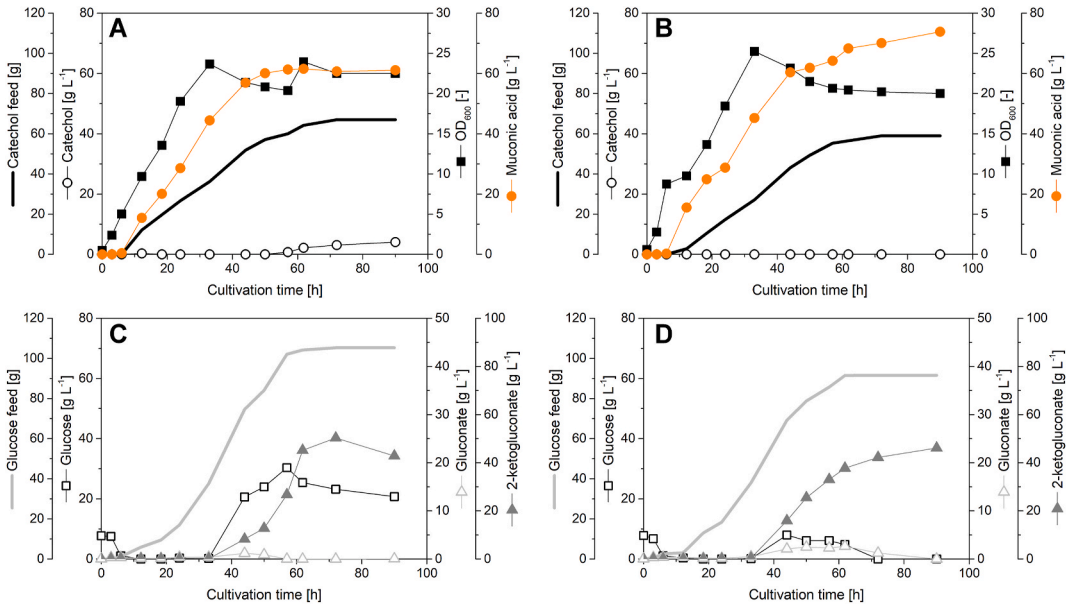

Fig. 9. Yield-optimized fed-batch production of *cis, cis*-muconate by metabolically engineered *Pseudomonas putida* MA-6 (A, C) and MA-11 (B, D). After depletion of the initial glucose at the end of the batch phase, the sugar was fed exponentially. Catechol pulses were added automatically, using a sudden increase in the pH value as a trigger, whereby the level of the aromatic in the broth was maintained below 0.5 mM n = 2.

25% reduced sugar requirement of the genome-reduced producer, shown here, suggests a striking economic advantage.

3.10. Synthesis of bio-PET from lignin-based MA

Finally, we used the novel strains to demonstrate the complete value chain. MA was purified from several fermentation batches, conducted here (see above). In total, this yielded 70 g of biobased MA (>98.5% purity) which was then used to synthesize the prominent PET monomer BHET (Fig. 10). A detailed description of the developed synthetic route is given in the supplementary file 1. In a first step, 70 g MA was isomerized under reflux into its *trans, trans*-isomer using molecular iodine (5% mol) as a catalyst. The reaction occurred at a reasonable yield of 84% and yielded 59 g TTMA with a purity of >98%. Subsequently, the *trans, trans*-muconic acid dimethyl ester (63 g DMMA) was obtained at 90% yield and >98% purity through esterification with methanol. using a catalytic amount of concentrated H_2SO_4. Next, a fraction of DMMA (23 g) was cyclized in a Diels-Alder reaction using ethylene gas as a dienophile at an overpressure of 8 bar (15 bar at the reaction temperature of 200 °C). After purification, 15 g of 1,4-dimethyl cyclohex-2-ene-1,4-dicarboxylate (DMCD) was obtained at >95% purity, corresponding to a yield of 57%. The subsequent oxidative aromatization of DMCD into dimethyl terephthalate (DMT) was realized in cyclohexane with 5% Pt/C as the catalyst. In this way, 9 g of cyclohexene dicarboxylate was converted into 1.8 g of 95% pure dimethyl terephthalate, corresponding to a yield of approximately 21%. DMT was transesterified into diethylene glycol terephthalate (BHET). Selective transesterification was achieved using *N,N*-diisopropylethylamine as reagent. On a larger scale, this approach converted 1.8 g of DMT into 1.2 g of BHET with a purity >98%, corresponding to 66% yield. As a final proof of concept, melt polymerization into PET was carried out using 1.2 g of the obtained monomer. Low pressure (20 mbar) was applied to distill off the released ethylene glycol. After 35 min, the reaction mixture solidified into a solid PET block. In total, 0.83 g of PET was formed, corresponding to 100% yield. Thermogravimetric analysis of the solid revealed a melting temperature range of 256–272 °C, which was in very good agreement with reference data, i.e., 109 °C for the monomer, 169 °C for the dimer, 199 °C for the trimer, and >250 °C for the PET polymer itself (Jog, 1995).

4. Conclusion

In this work, we demonstrate the first biobased PET from lignin-derived catechol and open up a promising green route to synthesize this most versatile bulk polymer from the world's most underutilized renewable (Pang et al., 2016). Notably, the chemical conversion largely

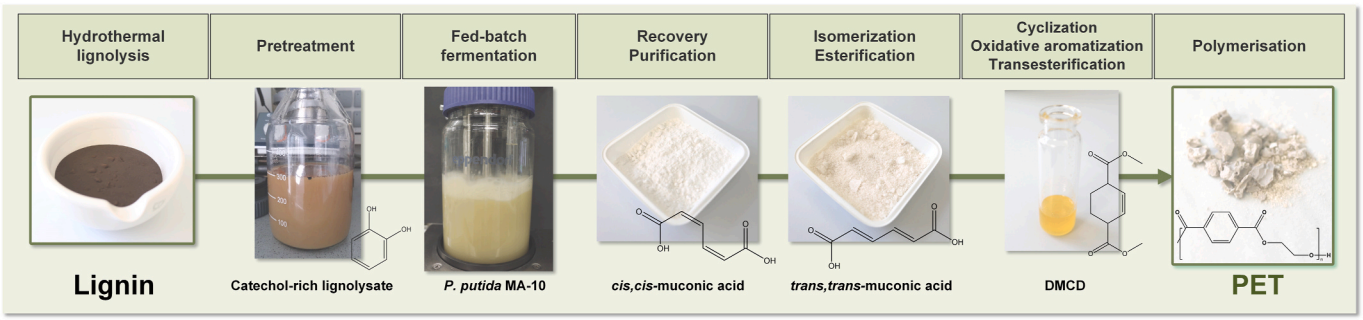

Fig. 10. Cascaded value chain from lignin to bio-PET. The cascaded process involves hydrothermal depolymerization of lignin into a catechol-rich hydrolysate (Kohlstedt et al., 2018), fermentative conversion of catechol into *cis, cis*-muconate by metabolically engineered *Pseudomonas putida*, purification of *cis, cis*-muconate from the broth, chemical conversion via several steps into the monomer diethylene glycol terephthalate, and final polymerization into PET.

relied on green solvents (MTHF, THF, MeOH) and catalysts (iodine, C). Lignin is a massively accumulating waste stream (Weiland et al., 2021) with promising advanced sustainability and secured availability when used for PET manufacturing. As the centerpiece of our cascaded value chain, we showed high-level fermentative conversion of catechol into MA using different *P. putida* strains. This achievement demonstrates relevance and feasibility because catechol is a major technical intermediate of the lignin industry and probably the most toxic intermediate (Becker and Wittmann, 2019). As example, catechol and alkylated derivatives display the most abundant monomers that is obtained during the depolymerization of various technical and isolated lignins, either using hydrothermal treatment in subcritical water (Islam et al., 2018), supercritical water (Wahyudiono et al., 2008) or base-catalyzed depolymerization (Katahira et al., 2016; Vigneault et al., 2007). Catechol is also among the most prevalent monomers, obtained through fast pyrolysis of lignin (van Duuren et al., 2020). Reductive catalytic fractionation of C-lignin even exclusively yields catechols (Stone et al., 2018).

One additional point to mention here is that catechol might be also relevant, when producing from "above" catechol substrates. In all cases, independent of the pathway, catechol displays the terminal pathway intermediate. Furthermore, catechol builds up during MA production from benzoate, an "above" catechol substrate (Kohlstedt et al., 2018), and it can be expected that this might also happen, when using aromatics mixtures and strains that are engineered for extended co-consumption. One should further note that mixtures of aromatics likely cause compounded toxicity effects, eventually superimposed during fermentation by inhibition from e. g. ammonium or oxygen availability which could contribute to catechol accumulation (Davis et al., 2015; Wittmann et al., 1995). A careful monitoring of MA production processes for the accumulation of catechol seems helpful to recognize and then alleviate such effects using e. g. adapted feeding strategies.

The superior efficiency of the fermentation process was enabled by the use of energy- and redox-optimized cell factories. As shown, the construction of these producers was inspired by the response of the microbe to catechol stress on the level of metabolic fluxes and their transcriptional regulation. In this regard, our data add valuable knowledge toward understanding the physiological needs of bacteria for lignin valorization (Granja-Travez et al., 2020; Moraes et al., 2018). The in-built robustness of the designed MA-producing strains MA-10 and MA-11, derivatives of the genome reduced chassis EM42, appeared essential for extra performance at the end of MA production processes with high product levels, the crunch time of fermentation. As shown, their use enabled attractive yields, rates, and titers, as well as reduced sugar costs. The increased tolerance to a range of other lignin-based aromatics, demonstrated for EM42, suggests that genome-reduced producers are attractive for different types of lignin and depolymerization strategies (Ragauskas et al., 2014; Rodriguez et al., 2017) and might generally add performance to this "field of dreams". Regarding the chemical synthesis of PET from MA, further catalytic optimization seems important to ultimately produce PET at high yield.

Author contributions

Michael Kohlstedt, Anna Weimer, Jessica Stolzenberger, Mirjam Selzer, Miguel Sanz, Laurenz Kramps: investigation, formal analysis; Michael Kohlstedt, Christoph Wittmann: visualization; Michael Kohlstedt, Anna Weimer, Fabia Weiland, Christoph Wittmann: drafting and revising the manuscript; Christoph Wittmann: design of study, conceptualization, supervision, editing, resources, funding acquisition.

Declaration of competing interest

Michael Kohlstedt, Jessica Stolzenberger, Mirjam Selzer, and Christoph Wittmann have filed patent applications on the use of lignin for bioproduction. The other authors declare that they have no competing interests.

Acknowledgments

The authors acknowledge Michel Fritz (Saarland University, Germany) for his support in analyses. We are grateful to Esteban Martinez-Garcia and Victor de Lorenzo (National Centre for Biotechnology, Madrid, Spain) for donating the strain *Pseudomonas putida* EM42. Christoph Wittmann acknowledges support by the German Ministry for Education and Research (BMBF) through the grants BioNylon (03V757) and LignoValue (031B0344A) and by the German Research Foundation (DFG) through the grant ePseudomonas within the Priority Programme "eBiotech" (SPP 2240). Fabia Weiland thanks the HaVo Foundation for funding her through a doctoral fellowship.

Appendix A. Supplementary data

Supplementary data to this article can be found online at https://doi.org/10.1016/j.ymben.2022.05.001.

References

Akkaya, O., Perez-Pantoja, D.R., Calles, B., Nikel, P.I., de Lorenzo, V., 2018. The metabolic redox regime of *Pseudomonas putida* tunes its evolvability toward novel xenobiotic substrates. mBio 9.

Almqvist, H., Veras, H., Li, K.N., Hidalgo, J.G., Hulteberg, C., Gorwa-Grauslund, M., Parachin, N.S., Carlquist, M., 2021. Muconic acid production using engineered *Pseudomonas putida* KT2440 and a guaiacol-rich fraction derived from Kraft lignin. ACS Sustain. Chem. Eng. 9, 8097–8106.

Barton, N., Horbal, L., Starck, S., Kohlstedt, M., Luzhetskyy, A., Wittmann, C., 2018. Enabling the valorization of guaiacol-based lignin: Integrated chemical and biochemical production of cis,cis-muconic acid using metabolically engineered *Amycolatopsis* sp ATCC 39116. Metab. Eng. 45, 200–210.

Bator, I., Wittgens, A., Rosenau, F., Tiso, T., Blank, L.M., 2020. Comparison of three xylose pathways in *Pseudomonas putida* KT2440 for the synthesis of valuable products. Front. Bioeng. Biotechnol. 7.

Becker, J., Klopprogge, C., Wittmann, C., 2008. Metabolic responses to pyruvate kinase deletion in lysine producing *Corynebacterium glutamicum*. Microb. Cell Factories 7, 8.

Becker, J., Klopprogge, C., Zelder, O., Heinzle, E., Wittmann, C., 2005. Amplified expression of fructose 1,6-bisphosphatase in *Corynebacterium glutamicum* increases *in vivo* flux through the pentose phosphate pathway and lysine production on different carbon sources. Appl. Environ. Microbiol. 71, 8587–8596.

Becker, J., Lange, A., Fabarius, J., Wittmann, C., 2015. Top value platform chemicals: bio-based production of organic acids. Curr. Opin. Biotechnol. 36, 168–175.

Becker, J., Wittmann, C., 2019. A field of dreams: lignin valorization into chemicals, materials, fuels, and health-care products. Biotechnol. Adv. 37.

Belda, E., van Heck, R.G.A., Lopez-Sanchez, M.J., Cruveiller, S., Barbe, V., Fraser, C., Klenk, H.P., Petersen, J., Morgat, A., Nikel, P.I., Vallenet, D., Rouy, Z., Sekowska, A., dos Santos, V.A.P.M., de Lorenzo, V., Danchin, A., Medigue, C., 2016. The revisited genome of *Pseudomonas putida* KT2440 enlightens its value as a robust metabolic chassis. Environ. Microbiol. 18, 3403–3424.

Benjamini, Y., Hochberg, Y., 1995. Controlling the false discovery rate - a practical and powerful approach to multiple testing. J. Roy. Stat. Soc. B 57, 289–300.

Bitzenhofer, N.L., Kruse, L., Thies, S., Wynands, B., Lechtenberg, T., Ronitz, J., Kozaeva, E., Wirth, N.T., Eberlein, C., Jaeger, K.E., Nikel, P.I., Heipieper, H.J., Wierckx, N., Loeschcke, A., 2021. Towards robust *Pseudomonas* cell factories to harbour novel biosynthetic pathways. Essays Biochem. 65, 319–336.

Blank, L.M., Ionidis, G., Ebert, B.E., Buhler, B., Schmid, A., 2008. Metabolic response of *Pseudomonas putida* during redox biocatalysis in the presence of a second octanol phase. FEBS J. 275, 5173–5190.

Brown, W., Turner, A.B., 1971. Applications of high-potential quinones. Part VII. The synthesis of steroidal phenanthrenes by double methyl migration. J. Chem. Soc. C Org. 2566–2572.

Bugg, T.D.H., Williamson, J.J., Alberti, F., 2021. Microbial hosts for metabolic engineering of lignin bioconversion to renewable chemicals. Renew. Sustain. Energy Rev. 152.

Cesati, R.R., Radeke, H.S., Pandey, S.K., Purohit, A., Robinson, S.P., 2015. Compositions, Methods and Systems for the Synthesis and Use of Contrast Agents.

Collias, I., Dimitris, Harris, M., Angela, Nagpa, V., Cottrell, W., Ian, Schultheis, W., Mikell, 2014. Biobased terephthalic acid Technologies: a literature review. Ind. Biotechnol. 10, 91–105.

Corona, A., Biddy, M.J., Vardon, D.R., Birkved, M., Hauschild, M.Z., Beckham, G.T., 2018. Life cycle assessment of adipic acid production from lignin. Green Chem. 20, 3857–3866.

Daddaoua, A., Krell, T., Alfonso, C., Morel, B., Ramos, J.L., 2010. Compartmentalized glucose metabolism in *Pseudomonas putida* is controlled by the PtxS repressor. J. Bacteriol. 192, 4357–4366.

Davis, R., Duane, G., Kenny, S.T., Cerrone, F., Guzik, M.W., Babu, R.P., Casey, E., O'Connor, K.E., 2015. High cell density cultivation of *Pseudomonas putida* KT2440 using glucose without the need for oxygen enriched air supply. Biotechnol. Bioeng. 112, 725–733.

del Castillo, T., Ramos, J.L., Rodriguez-Herva, J.J., Fuhrer, T., Sauer, U., Duque, E., 2007. Convergent peripheral pathways catalyze initial glucose catabolism in *Pseudomonas putida*: genomic and flux analysis. J. Bacteriol. 189, 5142–5152.

Ebert, B.E., Kurth, F., Grund, M., Blank, L.M., Schmid, A., 2011. Response of *Pseudomonas putida* KT2440 to increased NADH and ATP demand. Appl. Environ. Microbiol. 77, 6597–6605.

Frost, J.W., Miermont, A., Schweitzer, D., Bui, V., 2010. Preparation of Trans,trans Muconic Acid and Trans,trans-Muconates. Amyris, Inc, Emeryville, CA (US), US. US 8,426,639 B2.

Frost, J.W., Miermont, A., Schweitzer, D., V, B., Wicks, D.A., 2013. Terepthtalic and Trimellic Based Acids and Carboxylate Derivatives Thereof. Amyris, Inc., Emeryville, CA (US), US. US 8,367,858 B2.

Gentleman, R.C., Carey, V.J., Bates, D.M., Bolstad, B., Dettling, M., Dudoit, S., Ellis, B., Gautier, L., Ge, Y., Gentry, J., Hornik, K., Hothorn, T., Huber, W., Iacus, S., Irizarry, R., Leisch, F., Li, C., Maechler, M., Rossini, A.J., Sawitzki, G., Smith, C., Smyth, G., Tierney, L., Yang, J.Y., Zhang, J., 2004. Bioconductor: open software development for computational biology and bioinformatics. Genome Biol. 5, R80.

Geyer, R., 2020. Chapter 2 - production, use, and fate of synthetic polymers. In: Letcher, T.M. (Ed.), Plastic Waste and Recycling. Academic Press, pp. 13–32.

Giesselmann, G., Dietrich, D., Jungmann, L., Kohlstedt, M., Jeon, E.J., Yim, S.S., Sommer, F., Zimmer, D., Muhlhaus, T., Schroda, M., Jeong, K.J., Becker, J., Wittmann, C., 2019. Metabolic engineering of *Corynebacterium glutamicum* for high-level ectoine production: design, combinatorial assembly, and implementation of a transcriptionally balanced heterologous ectoine pathway. Biotechnol. J. 14, e1800417.

Goncalves, C.C., Bruce, T., Silva, C.D.G., Ferreira, E.X., Noronha, E.F., Carlquist, M., Parachin, N.S., 2020. Bioprospecting microbial diversity for lignin valorization: dry and wet screening methods. Front. Microbiol. 11.

Granja-Travez, R.S., Persinoti, G.F., Squina, F.M., Bugg, T.D.H., 2020. Functional genomic analysis of bacterial lignin degraders: diversity in mechanisms of lignin oxidation and metabolism. Appl. Microbiol. Biotechnol. 104, 3305–3320.

Hallsworth, J.E., Heim, S., Timmis, K.N., 2003. Chaotropic solutes cause water stress in *Pseudomonas putida*. Environ. Microbiol. 5, 1270–1280.

Hardy, G.P.M.A., Demattos, M.J.T., Neijssel, O.M., 1993. Energy-conservation by pyrroloquinoline quinol-linked xylose oxidation in *Pseudomonas putida* Nctc-10936 during carbon-limited growth in chemostat culture. FEMS Microbiol. Lett. 107, 107–110.

Hartmans, S., Smits, J.P., Vanderwerf, M.J., Volkering, F., Debont, J.A.M., 1989. Metabolism of styrene oxide and 2-phenylethanol in the styrene-degrading *Xanthobacter* strain 124x. Appl. Environ. Microbiol. 55, 2850–2855.

Hilt, G., Danz, M., 2008. Regioselective cobalt-catalyzed Diels-Alder reaction towards 1,3-disubstituted and 1,2,3-trisubstituted benzene derivatives. Synthesis 14, 2257–2263.

Hoffmann, S.L., Kohlstedt, M., Jungmann, L., Hutter, M., Poblete-Castro, I., Becker, J., Wittmann, C., 2021. Cascaded valorization of brown seaweed to produce l-lysine and value-added products using *Corynebacterium glutamicum* streamlined by systems metabolic engineering. Metab. Eng. 67, 293–307.

Imlay, J.A., 2013. The molecular mechanisms and physiological consequences of oxidative stress: lessons from a model bacterium. Nat. Rev. Microbiol. 11, 443–454.

Islam, M.N., Taki, G., Rana, M., Park, J.H., 2018. Yield of phenolic monomers from lignin hydrothermolysis in subcritical water system. Ind. Eng. Chem. Res. 57, 4779–4784.

Jayakody, L.N., Johnson, C.W., Whitham, J.M., Giannone, R.J., Black, B.A., Cleveland, N. S., Klingeman, D.M., Michener, W.E., Olstad, J.L., Vardon, D.R., Brown, R.C., Brown, S.D., Hettich, R.L., Guss, A.M., Beckham, G.T., 2018. Thermochemical wastewater valorization via enhanced microbial toxicity tolerance. Energy Environ. Sci. 11, 1625–1638.

Jog, J.P., 1995. Crystallization of polyethyleneterephthalate. J Macromol Sci R M C C35, 531–553.

Johnson, C.W., Abraham, P.E., Linger, J.G., Khanna, P., Hettich, R.L., Beckham, G.T., 2017. Eliminating a global regulator of carbon catabolite repression enhances the conversion of aromatic lignin monomers to muconate in *Pseudomonas putida* KT2440. Metab. Eng. Commun. 5, 19–25.

Johnson, C.W., Salvachua, D., Khanna, P., Smith, H., Peterson, D.J., Beckham, G.T., 2016. Enhancing muconic acid production from glucose and lignin-derived aromatic compounds via increased protocatechuate decarboxylase activity. Metab. Eng. Commun. 3, 111–119.

Juranovič, A., Kranjc, K., Polanc, S., Perdih, F., Kočevar, M., 2012. Diels–Alder reaction of fused pyran-2-ones with ethyl vinyl ether. Monatshefte für Chem. Chem. Month. 143, 771–777.

Katahira, R., Mittal, A., McKinney, K., Chen, X.W., Tucker, M.P., Johnson, D.K., Beckham, G.T., 2016. Base-catalyzed depolymerization of biorefinery lignins. ACS Sustain. Chem. Eng. 4, 1474–1486.

Kerridge, D., 1959. Synthesis of flagella by amino acid-requiring mutants of *Salmonella typhimurium*. J. Gen. Microbiol. 21, 168–179.

Khalil, I., Quintens, G., Junkers, T., Dusselier, M., 2020. Muconic acid isomers as platform chemicals and monomers in the biobased economy. Green Chem.

Koch, O., Götz, M.R., 2018. Mixtures of Cannabinoid Compounds, and Production and Use Thereof.

Kohlstedt, M., Sappa, P.K., Meyer, H., Maass, S., Zaprasis, A., Hoffmann, T., Becker, J., Steil, L., Hecker, M., van Dijl, J.M., Lalk, M., Mader, U., Stülke, J., Bremer, E., Völker, U., Wittmann, C., 2014. Adaptation of *Bacillus subtilis* carbon core metabolism to simultaneous nutrient limitation and osmotic challenge: a multi-omics perspective. Environ. Microbiol. 16, 1898–1917.

Kohlstedt, M., Starck, S., Barton, N., Stolzenberger, J., Selzer, M., Mehlmann, K., Schneider, R., Pleissner, D., Rinkel, J., Dickschat, J.S., Venus, J., J, B.J. H.v.D., Wittmann, C., 2018. From lignin to nylon: cascaded chemical and biochemical conversion using metabolically engineered *Pseudomonas putida*. Metab. Eng. 47, 279–293.

Kohlstedt, M., Wittmann, C., 2019. GC-MS-based C-13 metabolic flux analysis resolves the parallel and cyclic glucose metabolism of *Pseudomonas putida* KT2440 and *Pseudomonas aeruginosa* PAO1. Metab. Eng. 54, 35–53.

Kukurugya, M.A., Mendonca, C.M., Solhtalab, M., Wilkes, R.A., Thannhauser, T.W., Aristilde, L., 2019. Multi-omics analysis unravels a segregated metabolic flux network that tunes co-utilization of sugar and aromatic carbons in *Pseudomonas putida*. J. Biol. Chem. 294, 8464–8479.

Lai, B., Yu, S., Bernhardt, P.V., Rabaey, K., Virdis, B., Kromer, J.O., 2016. Anoxic metabolism and biochemical production in *Pseudomonas putida* F1 driven by a bioelectrochemical system. Biotechnol. Biofuels 9, 39.

Lange, A., Becker, J., Schulze, D., Cahoreau, E., Portais, J.C., Haefner, S., Schröder, H., Krawczyk, J., Zelder, O., Wittmann, C., 2017. Bio-based succinate from sucrose: high-resolution ^{13}C metabolic flux analysis and metabolic engineering of the rumen bacterium *Basfia succiniciproducens*. Metab. Eng. 44, 198–212.

Lee, S.-J., Peng, M.-L., Lee, J.-C., Chou, T.-S., 1992. 2,3-(Ethylenedisulfonyl)-1,3-butadiene, à versatile Diels-Alder diene and dienophile. Chem. Ber. 125, 499–504.

Li, G., Lu, S., 2019. Succinic Acid Furfural Diester Pesticide and Preparation Method and Application Thereof. Harbin University of Commerce, China, China. CN 109,369,578 B.

Lieder, S., Nikel, P.I., de Lorenzo, V., Takors, R., 2015. Genome reduction boosts heterologous gene expression in *Pseudomonas putida*. Microb. Cell Factories 14, 23.

Liu, Y., Hu, H., Wang, X., Zhi, S., Kan, Y., Wang, C., 2017. Synthesis of pyrrole via a silver-catalyzed 1,3-dipolar cycloaddition/oxidative dehydrogenative aromatization tandem reaction. J. Org. Chem. 82, 4194–4202.

Lou, Z.X., Wang, H.X., Rao, S.Q., Sun, J.T., Ma, C.Y., Li, J., 2012. *p*-Coumaric acid kills bacteria through dual damage mechanisms. Food Control 25, 550–554.

Macnab, R.M., 1996. Flagella and motility. In: Neidhardt, F.C. (Ed.), *Escherichia coli* and *Salmonella*: Cellular and Molecular Biology. ASM Press, Washington, D.C., pp. 123–145

Martínez-García, E., de Lorenzo, V., 2011. Engineering multiple genomic deletions in Gram-negative bacteria: analysis of the multi-resistant antibiotic profile of *Pseudomonas putida* KT2440. Environ. Microbiol. 13, 2702–2716.

Martinez-Garcia, E., Nikel, P.I., Aparicio, T., de Lorenzo, V., 2014. Pseudomonas 2.0: genetic upgrading of P. putida KT2440 as an enhanced host for heterologous gene expression. Microb. Cell Factories 13, 159.

Martínez-García, E., Nikel, P.I., Aparicio, T., de Lorenzo, V., 2014. *Pseudomonas* 2.0: genetic upgrading of *P. putida* KT2440 as an enhanced host for heterologous gene expression. Microb. Cell Factories 13, 159, 159.

McGroarty, E.J., Koffler, H., Smith, R.W., 1973. Regulation of flagellar morphogenesis by temperature: involvement of the bacterial cell surface in the synthesis of flagellin and the flagellum. J. Bacteriol. 113, 295–303.

Moraes, E.C., Alvarez, T.M., Persinoti, G.F., Tomazetto, G., Brenelli, L.B., Paixao, D.A.A., Ematsu, G.C., Aricetti, J.A., Caldana, C., Dixon, N., Bugg, T.D.H., Squina, F.M., 2018. Lignolytic-consortium omics analyses reveal novel genomes and pathways involved in lignin modification and valorization. Biotechnol. Biofuels 11.

Müller, P., Miao, Z., 1994. Synthesis of carbo- and heterocyclic cycloprop[f]indenes via cycloaddition of dienes to cyclopropenes. Helv. Chim. Acta 77, 1826–1836.

Nelson, K.E., Weinel, C., Paulsen, I.T., Dodson, R.J., Hilbert, H., Martins dos Santos, V.A. P., Fouts, D.E., Gill, S.R., Pop, M., Holmes, M., Brinkac, L., Beanan, M., DeBoy, R.T., Daugherty, S., Kolonay, J., Madupu, R., Nelson, W., White, O., Peterson, J., Khouri, H., Hance, I., Lee, P.C., Holtzapple, E., Scanlan, D., Tran, K., Moazzez, A., Utterback, T., Rizzo, M., Lee, K., Kosack, D., Moestl, D., Wedler, H., Lauber, J., Stjepandic, D., Hoheisel, J., Straetz, M., Heim, S., Kiewitz, C., Eisen, J., Timmis, K.N., Düsterhöft, A., Tümmler, B., Fraser, C.M., 2002. Complete genome sequence and comparative analysis of the metabolically versatile *Pseudomonas putida* KT2440. Environ. Microbiol. 4, 799–808.

Nikel, P.I., Chavarria, M., Fuhrer, T., Sauer, U., de Lorenzo, V., 2015. *Pseudomonas putida* KT2440 strain metabolizes glucose through a cycle formed by enzymes of the Entner-Doudoroff, Embden-Meyerhof-Parnas, and pentose phosphate pathways. J. Biol. Chem. 290, 25920–25932.

Nikel, P.I., Fuhrer, T., Chavarria, M., Sanchez-Pascuala, A., Sauer, U., de Lorenzo, V., 2021. Reconfiguration of metabolic fluxes in *Pseudomonas putida* as a response to sub-lethal oxidative stress. ISME J. 15, 1751–1766.

Nikel, P.I., Perez-Pantoja, D., de Lorenzo, V., 2016. Pyridine nucleotide transhydrogenases enable redox balance of *Pseudomonas putida* during biodegradation of aromatic compounds. Environ. Microbiol. 18, 3565–3582.

Nogales, J., García, J.L., Díaz, E., 2017. Degradation of aromatic compounds in *Pseudomonas*: a systems biology view. In: Rojo, F. (Ed.), Aerobic Utilization of Hydrocarbons, Oils and Lipids. Handbook of Hydrocarbon and Lipid Microbiology. Springer, Cham, pp. 1–49.

Oberhardt, M.A., Puchalka, J., dos Santos, V.A.P.M., Papin, J.A., 2011. Reconciliation of genome-scale metabolic reconstructions for comparative systems analysis. PLoS Comput. Biol. 7.

Pang, J.F., Zheng, M.Y., Sun, R.Y., Wang, A.Q., Wang, X.D., Zhang, T., 2016. Synthesis of ethylene glycol and terephthalic acid from biomass for producing PET. Green Chem. 18, 342–359.

Quek, L.-E., Wittmann, C., Nielsen, L.K., Krömer, J.O., 2009. OpenFLUX: efficient modelling software for ^{13}C-based metabolic flux analysis. Microb. Cell Factories 8, 25.

Ragauskas, A.J., Beckham, G.T., Biddy, M.J., Chandra, R., Chen, F., Davis, M.F., Davison, B.H., Dixon, R.A., Gilna, P., Keller, M., Langan, P., Naskar, A.K., Saddler, J. N., Tschaplinski, T.J., Tuskan, G.A., Wyman, C.E., 2014. Lignin valorization: improving lignin processing in the biorefinery. Science 344, 1246843.

Reining, B., Keul, H., Hocker, H., 2002. Block copolymers comprising poly(ethylene oxide) and poly (hydroxyethyl methacrylate) blocks: synthesis and characterization. Polymer 43, 3139–3145.

Rodriguez, A., Salvachúa, D., Katahira, R., Black, B.A., Cleveland, N.S., Reed, M., Smith, H., Baidoo, E.E.K., Keasling, J.D., Simmons, B.A., Beckham, G.T., Gladden, J. M., 2017. Base-catalyzed depolymerization of solid lignin-rich streams enables microbial conversion. ACS Sustain. Chem. Eng. 5, 8171–8180.

Roell, G.W., Carr, R.R., Campbell, T., Shang, Z., Henson, W.R., Czajka, J.J., Martin, H.G., Zhang, F., Foston, M., Dantas, G., Moon, T.S., Tang, Y.J., 2019. A concerted systems biology analysis of phenol metabolism in *Rhodococcus opacus* PD630. Metab. Eng. 55, 120–130.

Rohles, C.M., Glaser, L., Kohlstedt, M., Giesselmann, G., Pearson, S., del Campo, A., Becker, J., Wittmann, C., 2018. A bio-based route to the carbon-5 chemical glutaric acid and to bionylon-6,5 using metabolically engineered *Corynebacterium glutamicum*. Green Chem. 20, 4662–4674.

Rorrer, N.A., Nicholson, S., Carpenter, A., Biddy, M.J., Grundl, N.J., Beckham, G.T., 2019. Combining reclaimed PET with bio-based monomers enables plastics upcycling. Joule 3, 1006–1027.

Sadler, J.C., Wallace, S., 2021. Microbial synthesis of vanillin from waste poly(ethylene terephthalate). Green Chem. 23, 4665–4672.

Salvachua, D., Johnson, C.W., Singer, C.A., Rohrer, H., Peterson, D.J., Black, B.A., Knapp, A., Beckham, G.T., 2018. Bioprocess development for muconic acid production from aromatic compounds and lignin. Green Chem. 20, 5007–5019.

Schutyser, W., Renders, T., Van den Bosch, S., Koelewijn, S.F., Beckham, G.T., Sels, B.F., 2018. Chemicals from lignin: an interplay of lignocellulose fractionation, depolymerisation, and upgrading. Chem. Soc. Rev. 47, 852–908.

Schweigert, N., Zehnder, A.J.B., Eggen, R.I.L., 2001. Chemical properties of catechols and their molecular modes of toxic action in cells, from microorganisms to mammals. Environ. Microbiol. 3, 81–91.

Singh, A., Rorrer, N.A., Nicholson, S.R., Erickson, E., DesVeaux, J.S., Avelino, A.F.T., Lamers, P., Bhatt, A., Zhang, Y., Avery, G., Tao, L., Pickford, A.R., Carpenter, A.C., McGeehan, J.E., Beckham, G.T., 2021. Techno-economic, life-cycle, and socioeconomic impact analysis of enzymatic recycling of poly(ethylene terephthalate). Joule 5, 2479–2503.

Singh, R., Mailloux, R.J., Puiseux-Dao, S., Appanna, V.D., 2007. Oxidative stress evokes a metabolic adaptation that favors increased NADPH synthesis and decreased NADH production in *Pseudomonas fluorescens*. J. Bacteriol. 189, 6665–6675.

Smith, J.G., Welankiwar, S.S., Shantz, B.S., Lai, E.H., Chu, N.G., 1980. Synthetic routes to derivatives of polycyclic aromatic hydrocarbons using isobenzofurans as transient reactive intermediates. J. Org. Chem. 45, 1817–1824.

Smyth, G.K., 2004. Linear models and empirical bayes methods for assessing differential expression in microarray experiments. Stat. Appl. Genet. Mol. Biol. 3, Article3.

Sonoki, T., Takahashi, K., Sugita, H., Hatamura, M., Azuma, Y., Sato, T., Suzuki, S., Kamimura, N., Masai, E., 2018. Glucose-free *cis,cis*-muconic acid production via new metabolic designs corresponding to the heterogeneity of lignin. ACS Sustain. Chem. Eng. 6, 1256–1264.

Stephan, S., Heinzle, E., Wenzel, S.C., Krug, D., Müller, R., Wittmann, C., 2006. Metabolic physiology of *Pseudomonas putida* for heterologous production of myxochromid. Process Biochem. 41, 2146–2152.

Stone, M.L., Anderson, E.M., Meek, K.M., Reed, M., Katahira, R., Chen, F., Dixon, R.A., Beckham, G.T., Roman-Leshkoy, Y., 2018. Reductive catalytic fractionation of C-lignin. ACS Sustain. Chem. Eng. 6, 11211–11218.

Tam, L.T., Eymann, C., Albrecht, D., Sietmann, R., Schauer, F., Hecker, M., Antelmann, H., 2006. Differential gene expression in response to phenol and catechol reveals different metabolic activities for the degradation of aromatic compounds in *Bacillus subtilis*. Environ. Microbiol. 8, 1408–1427.

Tiso, T., Narancic, T., Wei, R., Pollet, E., Beagan, N., Schröder, K., Honak, A., Jiang, M., Kenny, S.T., Wierckx, N., Perrin, R., Avérous, L., Zimmermann, W., O'Connor, K., Blank, L.M., 2021. Towards bio-upcycling of polyethylene terephthalate. Metab. Eng. 66, 167–178.

Tiso, T., Sabelhaus, P., Behrens, B., Wittgens, A., Rosenau, F., Hayen, H., Blank, L.M., 2016. Creating metabolic demand as an engineering strategy in *Pseudomonas putida* - rhamnolipid synthesis as an example. Metab. Eng. Commun. 3, 234–244.

Tlemcani, L.L., Corroler, D., Barillier, D., Mosrati, R., 2008. Physiological states and energetic adaptation during growth of *Pseudomonas putida* mt-2 on glucose. Arch. Microbiol. 190, 141–150.

Toledano, A., Serrano, L., Labidi, J., 2012. Organosolv lignin depolymerization with different base catalysts. J. Chem. Technol. Biotechnol. 87, 1593–1599.

Tournier, V., Topham, C.M., Gilles, A., David, B., Folgoas, C., Moya-Leclair, E., Kamionka, E., Desrousseaux, M.L., Texier, H., Gavalda, S., Cot, M., Guémard, E., Dalibey, M., Nomme, J., Cioci, G., Barbe, S., Chateau, M., André, I., Duquesne, S., Marty, A., 2020. An engineered PET depolymerase to break down and recycle plastic bottles. Nature 580, 216–219.

van Duuren, J., de Wild, P.J., Starck, S., Bradtmoller, C., Selzer, M., Mehlmann, K., Schneider, R., Kohlstedt, M., Poblete-Castro, I., Stolzenberger, J., Barton, N., Fritz, M., Scholl, S., Venus, J., Wittmann, C., 2020. Limited life cycle and cost assessment for the bioconversion of lignin-derived aromatics into adipic acid. Biotechnol. Bioeng. 117, 1381–1393.

van Duuren, J.B., Wijte, D., Karge, B., dos Santos, V.A., Yang, Y., Mars, A.E., Eggink, G., 2012. pH-stat fed-batch process to enhance the production of cis, cis-muconate from benzoate by *Pseudomonas putida* KT2440-JD1. Biotechnol. Prog. 28, 85–92.

van Duuren, J.B.J.H., Puchałka, J., Mars, A.E., Bücker, R., Eggink, G., Wittmann, C., dos Santos, V.A.P.M., 2013. Reconciling in vivo and in silico key biological parameters of *Pseudomonas putida* KT2440 during growth on glucose under carbon-limited condition. BMC Biotechnol. 13, 93.

van Winden, W.A., Wittmann, C., Heinzle, E., Heijnen, J.J., 2002. Correcting mass isotopomer distributions for naturally occurring isotopes. Biotechnol. Bioeng. 80, 477–479.

Vardon, D.R., Franden, M.A., Johnson, C.W., Karp, E.M., Guarnieri, M.T., Linger, J.G., Salm, M.J., Strathmann, T.J., Beckham, G.T., 2015. Adipic acid production from lignin. Energy Environ. Sci. 8, 617–628.

Vardon, D.R., Rorrer, N.A., Salvachua, D., Settle, A.E., Johnson, C.W., Menart, M.J., Cleveland, N.S., Ciesielski, P.N., Steirer, K.X., Dorgan, J.R., Beckham, G.T., 2016. *cis, cis*-Muconic acid: separation and catalysis to bio-adipic acid for nylon-6,6 polymerization. Green Chem. 18, 3397–3413.

Varman, A.M., He, L., Follenfant, R., Wu, W.H., Wemmer, S., Wrobel, S.A., Tang, Y.J.J., Singh, S., 2016. Decoding how a soil bacterium extracts building blocks and metabolic energy from ligninolysis provides road map for lignin valorization. Proc. Natl. Acad. Sci. Unit. States Am. 113, E5802–E5811.

Vigneault, A., Johnson, D.K., Chornet, E., 2007. Base-catalyzed depolymerization of lignin: separation of monomers. Can. J. Chem. Eng. 85, 906–916.

Volke, D.C., Olavarria, K., Nikel, P.I., 2021. Cofactor specificity of glucose-6-Phosphate dehydrogenase isozymes in *Pseudomonas putida* reveals a general principle underlying glycolytic strategies in bacteria. mSystems 6.

Wahyudiono, Sasaki, M., Goto, M., 2008. Recovery of phenolic compounds through the decomposition of lignin in near and supercritical water. Chem. Eng. Process 47, 1609–1619.

Weiland, F., Kohlstedt, M., Wittmann, C., 2021. Guiding stars to the field of dreams: metabolically engineered pathways and microbial platforms for a sustainable lignin-based industry. Metab. Eng.

Werner, A.Z., Clare, R., Mand, T.D., Pardo, I., Ramirez, K.J., Haugen, S.J., Bratti, F., Dexter, G.N., Elmore, J.R., Huenemann, J.D., Peabody, G.L., Johnson, C.W., Rorrer, N.A., Salvachúa, D., Guss, A.M., Beckham, G.T., 2021. Tandem chemical deconstruction and biological upcycling of poly(ethylene terephthalate) to β-ketoadipic acid by Pseudomonas putida KT2440. Metab. Eng. 67, 250–261.

Wittmann, C., 2007. Fluxome analysis using GC-MS. Microb. Cell Factories 6, 6.

Wittmann, C., Heinzle, E., 2002. Genealogy profiling through strain improvement by using metabolic network analysis: metabolic flux genealogy of several generations of lysine-producing corynebacteria. Appl. Environ. Microbiol. 68, 5843–5859.

Wittmann, C., Kiefer, P., Zelder, O., 2004. Metabolic fluxes in *Corynebacterium glutamicum* during lysine production with sucrose as carbon source. Appl. Environ. Microbiol. 70, 7277–7287.

Wittmann, C., Zeng, A.P., Deckwer, W.D., 1995. Growth inhibition by ammonia and use of a pH-controlled feeding strategy for the effective cultivation of *Mycobacterium chlorophenolicum*. Appl. Microbiol. Biotechnol. 44, 519–525.

Wong, S.M., Mekalanos, J.J., 2000. Genetic footprinting with mariner-based transposition in *Pseudomonas aeruginosa*. Proc. Natl. Acad. Sci. U. S. A. 97, 10191–10196.

Xie, N.Z., Liang, H., Huang, R.B., Xu, P., 2014. Biotechnological production of muconic acid: current status and future prospects. Biotechnol. Adv. 32, 615–622.

Yuan, Q.Q., Huang, T., Li, P.S., Hao, T., Li, F.R., Ma, H.W., Wang, Z.W., Zhao, X.M., Chen, T., Goryanin, I., 2017. Pathway-consensus approach to metabolic network reconstruction for *Pseudomonas putida* KT2440 by systematic comparison of published models. PLoS One 12.

Zhang, H., Li, Z., Pereira, B., Stephanopoulos, G., 2015. Engineering *E. coli-E. coli* cocultures for production of muconic acid from glycerol. Microb. Cell Factories 14, 134.